MAGNETOSTRICTIVE DEVICES

1. INTRODUCTION

Magnetostrictive materials convert magnetic energy to mechanical energy, and vice versa. As a magnetostrictive material is magnetized, it deforms or strains. Conversely, when a magnetostrictive material is subjected to stresses, its magnetization changes. The bidirectional coupling between the magnetic and mechanical states of a magnetostrictive material provides a transduction mechanism that is used for actuation and sensing. The associated changes in material properties can also be beneficial, for example, to magnetically adjust the elastic modulus of a magnetostrictive material. Magnetostriction is an inherent material property that literally means "magnetically induced strain."

The history of magnetostriction began in the early 1840s when James Prescott Joule (1818–1889) positively identified the change in length of an iron sample as its magnetization changed. This effect, known as the Joule effect, is the most common mechanism employed in magnetostrictive actuators. A transverse change in dimensions accompanies the length change produced by the Joule effect, so the net volume change of the material is zero. The reciprocal effect, in which application of a stress causes a change in magnetization, is known as the Villari effect. The Villari effect is useful for sensor design.

The magnetostrictive effect is not limited to linear magnetostriction; however, it is present in all material tensor directions. For instance, the Wiedemann effect is the twisting that results from a helical magnetic field. The inverse Wiedemann effect, also known as the Matteuci effect, refers to the generation of a magnetic field due to shear stresses. This effect is useful for magnetoelastic torque sensing (1,2).

Early uses of magnetostrictive materials included telephone receivers, hydrophones, magnetostrictive oscillators, torque meters, and scanning sonar. The first telephonic receiver, tested by Philipp Reis in 1861, was based on magnetostriction (3). These applications were developed with nickel and other magnetostrictive materials that exhibit bulk saturation strains of less than 100 microstrain (100×10^{-6} change in length per original length). The development of terbium–iron–dysprosium alloys in the 1970s capable of generating over 1000 microstrain at room temperature, also known as "giant" magnetostrictive materials, generated renewed interest in magnetostrictive transducer technologies. These alloys, credited to the US Naval Ordnance Laboratory (NOL) under the name Terfenol-D (Ter = terbium, Fe = iron, NOL, D = dysprosium), became commercially available in the 1980s. The most recent class of magnetostrictive materials, based on iron–gallium alloys or Galfenol (also developed at NOL), exhibit moderate magnetostriction (≈400 microstrain) along with mechanical robustness not present in the mechanically brittle Terfenol-D alloys.

Commercial uses for magnetostrictive devices have emerged since the early 1990s, for example, a motor that is capable of converting 30 kW of electrical power to mechanical ultrasonic power at about 20 kHz (4) and flextensional underwater sonar projectors that can be driven to a source level of 212 dB (refer to 1 μPa at 1 m) (5). A high force test rig for use by the US Air Force in fatigue testing of jet engine turbine blades produces broadband forces from 200 to 2000 Hz with peak-to-peak force of 14 kN at 2 kHz (6). Taking advantage of the fast dynamic response of Terfenol-D, the manufacturer of Terfenol-D in the United States (Etrema Products (8)) developed an active machining system for production of oval pistons for small internal combustion engines. An ultrasonic fuel injector driven by a Terfenol-D element was developed (7). The high-frequency and high-power vibration generated by magnetostrictive materials has been used to prevent the clogging of nozzles in paper production and to improve mechanical screening efficiency in mining (8). Magnetostrictive devices have also been used in the entertainment industry. The Terfenol-D soundbugs, developed by FeONIC, can turn walls, windows, or other flat surfaces into speakers (9). Being a more recent material technology, Galfenol alloys have not been implemented commercially at a significant scale yet. Example research applications include the deposition of these ductile alloys epitaxially on a Si or Cu substrate for development of acoustic sensors (10) and force sensors based on thin Galfenol films (11).

2. MAGNETOSTRICTIVE MATERIALS

All ferromagnetic materials exhibit magnetostriction; however, in many materials, its magnitude is small. In the early 1970s, the search for a material capable of large magnetostriction at room temperature grew out of the discovery that the rare earth elements terbium and dysprosium exhibit magnetostriction (basal plane strains) on the order of 1% at cryogenic temperatures. From 1971 to 1972, Clark and Belson of the NSWC (Naval Surface Warfare Center) (12) and Koon, Schindler, and Carter of the NRL (Naval Research Laboratory) (13) independently and almost simultaneously discovered the extremely large room-temperature magnetostriction of the rare earth–iron, RFe_2, compounds.

Partial substitution of other rare earths, such as dysprosium, for terbium in the Tb–Fe compound resulted in improvements in magnetic and mechanical properties. The nominal stoichiometry of Tb–Dy–Fe that became known as Terfenol-D is $Tb_xDy_{1-x}Fe_y$, where x = 0.27–0.3 and y = 1.92–2.0. Small changes in x and y can result in significant changes in the magnetic and magnetostrictive properties of the material. Decreasing y below 2.0 dramatically reduces the brittleness of the compound, but reduces the magnetostrain. Increasing x above 0.27 does not significantly affect the magnetostrain, but reduces the magnetocrystalline anisotropy, which effectively allows for increased magnetostriction at lower fields and more efficient energy transduction.

Nominal maximum magnetically- induced longitudinal strain at room temperature for various materials are shown in Table 1. Nickel has a negative magnetostriction since it shortens in the presence of a magnetic field,

J. Webster (ed.), *Wiley Encyclopedia of Electrical and Electronics Engineering*.
DOI: 10.1002/047134608X.W4549.pub2

Table 1. Nominal Magnetically Induced Strain of Selected Magnetostrictive Materials

Material	Magnetostriction (μl/l)
Iron (14)	−9
Nickel (15)	−40
Alfenol (16)	150
Metglas 2605SC (17)	40
Terfenol-D (8)	1400
Galfenol (31)	400

whereas other materials including Terfenol-D exhibit positive magnetostriction. In the case of iron, the magnetostriction changes from positive to negative, known as the Villari reversal, as the field is increased (14).

Clark et al. (18) developed a magnetostrictive material based on amorphous metal, produced by extremely rapid cooling at rates around 1×10^6 °C/s of iron, nickel, or cobalt together with one or more of the elements silicon, boron, and phosphorus. These alloys, known commercially as Metglas (metallic glass), have been processed to achieve very high coupling coefficients, on the order of 0.95, and are commonly produced in thin ribbon geometries. Metglas is typically used for sensing applications and for converting mechanical or acoustical energy into electrical energy. The ease with which they can be magnetized and demagnetized and the low core losses of these alloys constitute a distinct set of magnetic properties that have motivated investigation of metallic glasses and their applications (20).

Giant magnetostrictive materials are currently available in a variety of forms, including thin films, powder composites, and monolithic solid drivers. Reviews of giant thin film magnetostrictive material are available (2,21,22). Giant magnetostrictive particle composites (GMPCs) consist of a powdered magnetostrictive material (often Terfenol-D) solidified in a resin or elastomeric matrix (23). GMPCs have the advantage that the nonelectrically conducting matrix material can be used to reduce eddy current losses associated with AC operation, while also being conducive to manufacture by casting in various geometries with advantageous mechanical properties such as ductility and machinability. Furthermore, devices using a driver element made with GMPCs as opposed to monolithic material may avoid the need for prestress mechanisms and the bulky permanent magnets needed for biased AC operation. The major disadvantage of GMPCs is a reduction in output strain and strain rates related to the matrix–Terfenol-D composition ratio (23–26).

Terfenol-D has been sputtered to form amorphous thin films (27) and has been doped with holmium to minimize magnetic hysteresis losses (28). Another application is magnetomemory materials that combine the magnetostrictive behavior of ferroelectric materials with the high-strain attributes found in shape memory alloys. Currently, the Fe–Pd–Co magnetomemory system exhibits magnetostriction several times that of the best giant magnetostrictive materials. Devices based on magnetomemory may provide significant advances in magnetostrictive sensing (29,30).

The iron–gallium alloys, or Galfenol ($Fe_{1-x}Ga_x, 0.13 \leq x \leq 0.24$), exhibit moderate magnetostriction (31) along with a relatively low hysteresis loss, high tensile strength (500 MPa), moderate corrosion resistance (32), and a high Curie temperature (700 °C) (31). Galfenol can be welded, forged, rolled, machined by conventional means, and deposited to form nanoscale or microscale fibers or films. In combination, these properties are unique in relation to Terfenol-D and other conventional active materials.

Addition of Co to binary Galfenol increases the Curie temperature but reduces magnetostriction (33). Alloying V, Al, or Cr with binary Galfenol improves the material's tensile strength and ductility, but Al–Galfenol alloys exhibit much lower magnetostriction (34). Recent Galfenol steel in which gallium is alloyed with carbon steel (35) is less expensive and exhibits improved malleability (36). Other iron alloys such as Fe–Al (16) and Fe–Be (37) have also been considered. However, they exhibit relatively small magnetostriction and the beryllium-containing materials are toxic.

For this survey of magnetostrictive devices, nickel, Terfenol-D, and Galfenol will be emphasized, as these are the most common commercially available materials used in magnetostrictive transducer applications.

3. MAGNETOSTRICTIVE DEVICE TRANSDUCTION BASICS

Magnetostrictive transducers operate on the simultaneous conversion of electromagnetic and magnetomechanical energies. A wound wire solenoid is used for conversion between electric and magnetic energies, and a magnetostrictive material is used as the transducer driver to convert between magnetic and mechanical energies. For actuation, passing a current through the solenoid converts electrical energy into magnetic energy. Maxwell's equations can be used to show that the magnetic field seen by the magnetostrictive driver is proportional to the current in the solenoid. The magnetic energy generated by the solenoid simultaneously magnetizes and produces strain in the magnetostrictive core. This same device can also be used as a sensor. Application of a sufficient force to strain the transducer magnetostrictive driver will produce a change in the magnetization of the driver. In turn, this changing magnetic energy can be measured directly with a Hall probe or, as can be shown by using the Faraday–Lenz law, it can be converted to electrical energy in the form of an induced voltage in the solenoid and then measured. A common magnetostrictive device configuration is sketched in Figure 1.

Figure 2a shows room-temperature flux density data for polycrystalline $Fe_{18.6}Ga_{18.4}$ driven with a 0.1 Hz magnetic field at several fixed stress values. The field-induced strain, or magnetostriction, versus applied magnetic field "butterfly" curves measured under the same conditions are shown in Figure 2b. Figures 2c and d show the flux density and strain versus low-frequency (1 Hz) AC stress inputs for the same Galfenol material. The magnetic field–strain curves are zeroed after applying constant bias stresses,

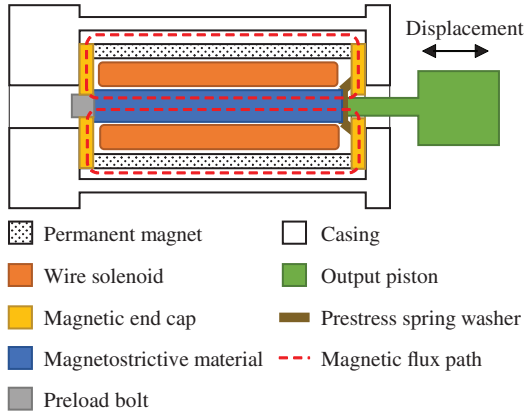

Figure 1. Components of basic magnetostrictive devices: magnetostrictive driver, magnetic end caps, permanent magnet, wound wire solenoid, magnetic circuit, and prestress mechanism.

while other curves are zeroed at no bias fields or bias stresses. Like Terfenol-D, Galfenol exhibits a rich performance space for actuation and sensing as a function of magnetic fields and stresses, although with less hysteresis than Terfenol-D.

The efficiency with which a magnetostrictive material converts magnetic energy to mechanical and vice versa is often used as a key attribute to quantify the performance of a magnetostrictive device. It is emphasized, however, that the design of high-performance magnetostrictive transducers also requires attention to the efficiency of conversion between electrical energy and magnetic energy. Although the practical input signals are voltage and current, it is the resulting magnetic field that generates the necessary magnetization of the magnetostrictive driver. This requires careful design of the transducer magnetic circuit, including incorporation of a closed magnetic flux return path. This is a task that is typically undertaken with finite-element (FE) analysis tools.

Furthermore, careful matching of the system power supply to the input impedance of the transducer needs to be considered when optimizing overall system efficiency. The power supply rating in Watts is equal to voltage times amperes and is given based on use with a specific load. Electrostrictive transducer technologies, based on piezoelectric and ferroelectric transduction, are electrically capacitive and as such they require high-voltage, low-current sources (on the order of 1000 V and microamperes). Magnetostrictive transducers, on the other hand, are electrically inductive requiring moderate voltages (less than 100–200 V) and relatively high currents (up to tens of amperes) for similar force outputs. Standard audio amplifiers can be effectively used to drive magnetostrictive devices.

Magnetostrictive materials have a fast dynamic response (39). In practice, the dynamic response of magnetostrictive devices is restricted to the low ultrasonic range (≤100 kHz) due to AC losses (magnetic hysteresis and eddy currents) and device-specific mechanical and electrical resonances.

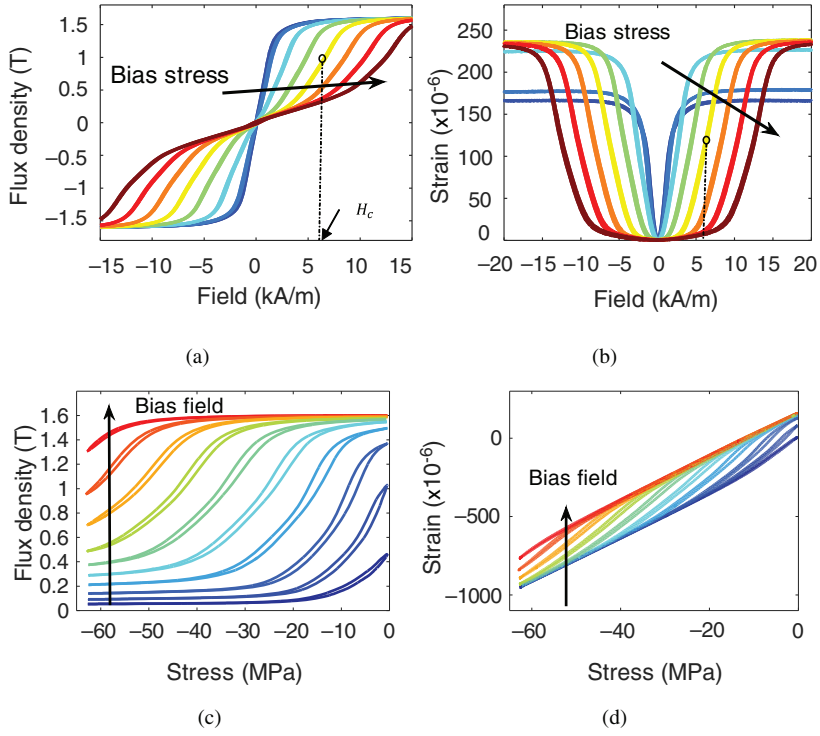

Figure 2. Actuation response of solid Galfenol ($Fe_{18.6}Ga_{18.4}$) for mean bias stresses of 0.00, –1.64, –10.23, –20.44, –30.65, –40.88, –51.10, and –61.31 MPa: (a) flux density versus field, and (b) actuation strain versus field (38); major loop sensing response of the same sample for mean bias fields of 0.73, 1.42, 2.41, 3.88, 5.50, 7.17, 8.84, 10.51, 12.19, and 13.76 kA/m: (c) flux density versus stress, and (d) strain versus stress. (38) All measurements were conducted at room temperature.

4. MAGNETOELASTIC EFFECT

The magnetostrictive process relating the magnetic and mechanical material states can be described with two coupled linear equations:

$$\epsilon = \sigma / E_y^H + d_{33}^* H \tag{1a}$$

$$B = d_{33}\sigma + \mu^\sigma H \tag{1b}$$

These equations assume isothermal conditions and linear (Joule) magnetostriction. Incorporation of other orientations is possible by formulating these equations in tensor form. The mechanical parameters are strain (ϵ), stress (σ), and Young's modulus at constant applied magnetic field (E_y^H); the magnetic parameters are applied magnetic field (H), magnetic induction (B), and permeability at constant stress (μ^σ); and the two piezomagnetic coefficients are $d_{33} = d\epsilon/dH|_\sigma$ and $d_{33}^* = dB/d\sigma|_H$.

Equation 1a indicates that the strain of a magnetostrictive element changes with stress and applied magnetic field. First, looking at the applied stress σ, when a stress is applied to a magnetostrictive sample, it will strain. If the field H is held constant and the stress varied, the material will contract if the stress is compressive and will expand if the stress is tensile. The magnitude of the effect is scaled by the inverse of the material's elastic modulus E_y^H. Next, an applied magnetic field H can also change the sample's length. If the stress is held constant, the effect of H in the strain is proportional to the applied field scaled by the piezomagnetic coefficient d_{33}. The elastic modulus and the piezomagnetic coefficients vary from one magnetostrictive material to the next and often vary with operating conditions. They need to be measured under carefully controlled electrical and mechanical boundary conditions. Similarly, the magnetic induction B will also vary with stress and applied field per equation 1b.

Figure 3 illustrates the interaction between magnetic moments (conceptually represented by elliptical magnets) and applied mechanical loads (represented by a spring and mass). Application of a negative saturation field ($-H_S$) has the same effect as a positive saturation field ($+H_S$), rotating the moments so that the material expands against the load and the magnetic induction reaches a maximum, saturation value. When no field is applied ($H = 0$), the mass load forces the magnets to collapse, resulting in zero net magnetic induction and the shortest material length. At intermediate fields ($-H_C$ and $+H_C$), the magnetic moment rotation and load are in an intermediate state where the magnetic field attempts to align the moments longitudinally and the mechanical load attempts to collapse the moments. Figure 3f shows the flux lines associated with alignment of the magnetic domains in the magnetostrictive driver.

A static compressive load is supplied in Figure 1 by a spring washer to prevent the magnetostrictive driver from undergoing tensile stress and potentially separating from the output rod. The dynamic forces arising during AC operation could have the effect of cracking the driver. This is particularly important for Terfenol-D due to its limited tensile strength. It has been shown that annealing of Galfenol can create sufficient internal prestresses (−200 to

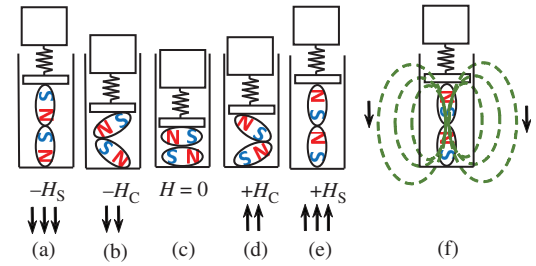

Figure 3. (a)–(e) Simplified representation of a magnetostrictive material for different magnetic field values. (f) Illustration of magnetic flux lines.

50 MPa) such that an external preload mechanism is not necessary (42). A static magnetic field or magnetic bias (H_c) is typically employed to create a static magnetization state and center operation in the high-slope regions (burst regions) where a small change in input field generates a large, approximately linear response. For instance, a bias field H_C of 6.17 kA/m and a prestress of −30.65 MPa are able to shift the static state to the center of the burst region, as illustrated by the black dots in Figure 2a and b. The bias field is often supplied by a permanent magnet as shown in Figure 1.

5. MAGNETOSTRICTIVE ACTUATORS

Magnetostrictive actuator designs are distinguished by their configuration and use of the magnetostrictive driver. Common transducer classifications can be found in the literature (43,44). In most cases, the Joule effect in a magnetostrictive element is employed to produce a longitudinal vibration in rods or radial vibrations of tubes or rings. The most common design is the longitudinal vibrating Tonpilz in which a magnetostrictive rod provides axial output (43). The tube-and-plate or tube-and-cone transducers use 1/4 wavelength magnetostrictive tubes to excite blocks tuned to transfer mechanical power to the surrounding medium efficiently. Other designs employ a number of magnetostrictive elements fitted end to end to form a ring or polygon (45). The simultaneous longitudinal excitation of the elements causes the ring's diameter to oscillate. The flextensional design (44) employs a longitudinal vibrating magnetostrictive element to excite an arched membrane, commonly an oval-shaped shell. Transducer designs have also been based on other magnetostrictive effects, such as the Wiedemann effect twisting pendulum (2).

Prior to the 1940s, the materials conventionally used for many transducer applications were the magnetostrictive elements nickel, cobalt, iron, and their alloys permendur, permalloy, and others. In the 1940s and 1950s, the emergence of piezoelectric ceramics barium titanate and lead zirconate titanate (PZT) led to higher efficiency transducer designs. The twofold increase in coupling coefficient of PZT over that of nickel provided higher transducer acoustic efficiencies and larger output powers in a number of applications. With the development of giant magnetostrictive materials in the 1970s, even higher transducer efficiencies are now achievable. The superiority of Terfenol-D over

piezoelectrics in high-power applications has been extensively demonstrated. Moffett et al. (46) present a theoretical comparison of the power-handling capability of Terfenol-D and PZTs. Moffett and Clay (47) later demonstrated the superior performance of Terfenol-D over PZT in a barrel-stave flextensional transducer in which the active motor was either Terfenol-D or PZT, with the rest of the device design otherwise unchanged. The Terfenol-D transducer had an FOM (figure of merit) of 60 W/(kgkHzQ), where Q is the quality factor, about four times that of the PZT transducer, and an 8 dB higher source level throughout a wider frequency bandwidth. Akutsu (48) reported a comparison of displacement versus output force relationships between PZT and Terfenol-D. Galfenol actuators have been shown to achieve a maximum energy density of around 3 kJ/m^3, but at limited strokes (49).

5.1. Device Performance

Magnetostrictive transducer performance has been quantified in several ways. The technique selected usually depends on several factors, including the intended use of the transducer and allowable resources. Performance quantification must involve analysis of the material properties under as-run conditions, that is, material properties of the active driver element based on measurements taken in the transducer under loads typical of a given application.

Magnetostrictive material properties are intrinsically related to the material magnetization, stress, and temperature distribution in the transducer. This relationship is strongly coupled, so changes in operating parameters affect material properties and vice versa (50). Typical material properties considered when analyzing magnetostrictive transducers include Young's modulus, mechanical quality factor, magnetic permeability, saturation magnetization and magnetostriction, magnetomechanical or piezomagnetic coefficient, and magnetomechanical coupling factor. Measurements of a transducer performance provide magnetoelastic parameters that are characteristic of both the magnetostrictive driver and the transducer itself. For instance, the magnetomechanical coupling factor quantifies the ratio of the coupled magnetic–elastic energy over the squared root of the product of the individual energies:

$$k = \frac{G_{\text{me}}}{\sqrt{G_{\text{m}} G_{\text{e}}}} = \frac{\sigma d_{33} H}{\sqrt{\mu^{\sigma} H^2 \sigma^2 / E_y^H}} = \frac{d_{33}}{\sqrt{\mu^{\sigma} / E_y^H}} \qquad (2)$$

When considering not just a magnetostrictive driver but a complete transducer, the magnetic and electric components have the effect of reducing the magnetomechanical coupling factor below that for the driver alone (40). On the other hand, the saturation magnetization and magnetostriction are properties of the driver material itself, not the transducer. Calculation of other material properties can be found in Reference 41 and 51–53.

To illustrate, we discuss in the following sections six key transducer performance indicators: (i) strain-applied field ($\epsilon - H$) characteristic curve, (ii) transducer electrical impedance mobility loops, (iii) transducer-blocked force, (iv) output energy and energy densities, (v) output power limitations, and (vi) figures of merit.

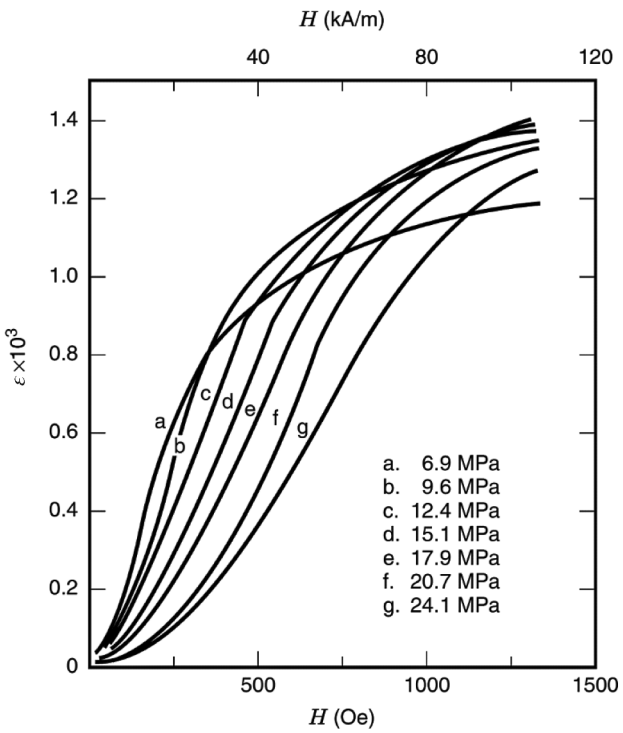

Figure 4. Strain-applied magnetic field relationship at 0.7 Hz and no magnetic bias (54).

Strain-Field Characteristic Curve. Static or quasi-static strain versus magnetic field curves are useful for performance and characterization. The magnetic field intensity is, for a given input current, determined by knowledge of the solenoid characteristics, and the mechanical output is measured with displacement sensors such as an LVDT (linear variable differential transformer). Typical strain measurements at different mechanical preloads are shown in Figure 4. A strain-applied field characteristic curve aids in choosing the optimum polarization field for achieving quasi-linear performance and for avoiding frequency doubling. Additionally, it can be used to estimate d_{33} coefficients.

Of the two linear constitutive piezomagnetic equations, equation 1b implies a definition for the strain coefficient, $d_{33} = [\partial\epsilon/\partial H]_{\sigma}$, which can be calculated from measurements such as those of Figure 4. Given the nonlinear and saturated response exhibited by the data, d_{33} can be estimated from the slope of a straight line drawn over the steepest region of the curve, often known as the "burst" region. By forgoing the last 10% of achievable strain at the saturation and low field ends of the curve, much higher efficiency performance can be achieved. Trade-offs in quantifying a d_{33} based on measured data arise, whereby if additional displacement is required (assuming space and cost constraints allow for it), one may opt for using a longer sample operating in the burst region rather than driving a shorter sample to saturation. This would provide two device designs using drivers of the same magnetostrictive material with potentially very different d_{33} coefficients.

This method for characterization of d_{33}, however, should be interpreted for use as measured (i.e., a DC measure of the transducer output). The differential values of d_{33} vary not only with H and σ (see Figures 2 and 4) but also with the magnetic bias, stress distribution in the material, and operating frequency (53,54). Hence, the strain-field characteristic curve is of little use in assessing transducer dynamic operation, where the preceding factors play a significant role. In such cases, methods based on dynamic excitation of the transducer are preferred (53).

Transducer Electrical Impedance Mobility Loops. The total transducer electrical impedance, the electrical voltage measured per input current as a function of frequency, is important for transducer design, analysis, and control. As discussed in detail by Hunt and Blackstock (3) and Rossi and Roe (55) among others, the electrical impedance is the sum of blocked and mobility impedances. The blocked impedance is the voltage per current associated with a transducer in which the output motion is restricted to zero, or "blocked". The mobility impedance is the difference in the total (measured) and blocked impedances and is a result of "mobility" or the force and velocity on the mechanical side of the vibrating transducer.

One use of impedance function information is to obtain fundamental resonant and antiresonant frequencies and the two associated elastic moduli for the magnetostrictive transducer driver. The resonant condition occurs when the magnitude of the mobility component of the measured impedance is maximum and is represented by the diameter of the mobility impedance loop in the Nyquist representation (56). The resonant frequency f_r is associated with the open-circuit (constant field) elastic modulus of the material E_y^H so that $f_r \propto \sqrt{E_y^H}$. Similarly, the maximum-diameter point of the electrical admittance loop ($Y_e = 1/Z_e$) represents the antiresonant frequency f_a associated with the short-circuit (constant induction) elastic modulus E_y^B. This relationship is such that $f_a \propto \sqrt{E_y^B}$.

The short-circuit modulus E_y^B represents the stiffest material condition, which occurs when all available magnetic energy has been transduced into elastic potential energy. When energy is transferred from the elastic to the magnetic side, the effective modulus decreases to the value E_Y^H. The two elastic moduli are related by the magnetomechanical coupling factor k ($0 \le k \le 1$) (57):

$$E_y^H = (1 - k^2)E_y^B \tag{3}$$

Similarly, the intrinsic or uncoupled magnetic permeability μ^σ in equation 1 is reduced to a value corresponding to the constant strain permeability μ^ϵ because of the energy conversion from the magnetic to the elastic side. Clark (57) provided further details and proved, through energy considerations, that both permeabilities are also related by k,

$$\mu^\epsilon = (1 - k^2)\mu^\sigma \tag{4}$$

Utilizing the simplified construct in Figure 3, holding the magnetic induction B constant while allowing σ and H to vary implies that the ellipses will not rotate, staying locked at fixed orientations. Hence, the transducer will appear stiffer to an external force than if H was held constant, but B and σ were allowed to vary. Alternatively, holding strain ϵ constant while varying H limits the potential change in B; thus, the material looks less permeable under operating conditions of constant strain than constant stress.

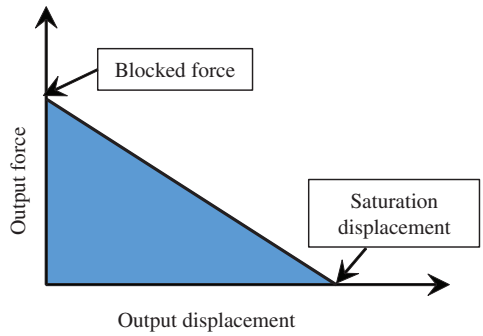

Figure 5. Representation of a linearized force versus displacement characteristic curve.

Ultimately, the electrical impedance provides information on how the energy is transferred between the magnetic and mechanical domains of a transducer. Knowledge of resonances f_r and f_a permits calculation of elastic moduli, magnetic permeabilities, and the magnetomechanical coupling factor (58).

Blocked Force. Figure 5 illustrates the static characteristic force versus displacement relationship of a magnetostrictive transducer. Under linearized conditions obtained under a bias magnetic field and prestress, as described by equation 1 it can be shown that the relationship is a straight line, although this is not the case in practice under high-signal conditions. As the transducer tries to do work against an increasing load force, its output displacement decreases. The blocked force is defined as the load against which the transducer can no longer work. At this load, the transducer displacement is reduced to zero, and the transducer output is blocked. At the other end of the load curve, if the load force is zero, the transducer will be able to elongate to its maximum (saturated) displacement. This condition is referred to as free displacement.

Under blocked conditions, $\epsilon = 0$ and equation 1 yields

$$\sigma = -d_{33}^* H E_y^H \tag{5}$$

where σ is the stress exerted by the load on the magnetostrictive driver. This stress is equal and opposite to the stress exerted by the driver on the load, which for a driver with cross-sectional area A gives an expression for the blocked force of the form:

$$F_B = d_{33}^* H E_y^H A \tag{6}$$

Because the saturation displacement u_H is achieved at zero force ($\sigma = 0$), equation 1 implies

$$u_H = d_{33}^* H L \tag{7}$$

where L is the length of the driver. Combination of equations 6 and 7 gives that the blocked force is

$$F_B = \frac{u_H}{L} E_y^H A \tag{8}$$

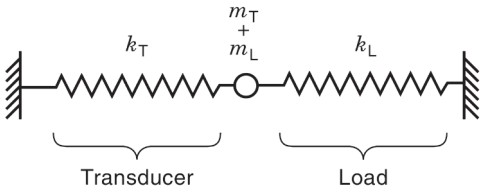

Figure 6. Schematic representation of an actuator of stiffness k_T loaded with an elastic load of spring constant k_L.

which can be expressed as the product of stiffness and displacement:

$$F_B = k_T u_H \tag{9}$$

with $k_T = E_y^H A/L$ representing the stiffness of the magnetostrictive transducer element. Equations 7 and 8 thus define the extreme points of the load curve (Figure 5), that is, the free displacement and blocked force, respectively. Defining the saturation strain as $\epsilon_s = d_{33}H$, the blocked force becomes $F_B = E_y^H A\epsilon_s$, which only depends on material properties and the cross-sectional area. In contrast, the maximum deflection depends on a material property and driver length.

Output Energy and Energy Densities. A linear elastic load of stiffness k_L is assumed to act on a Terfenol-D driver of stiffness k_T, as depicted in Figure 6. Since there is no energy loss, the potential energy applied to the load is

$$E_M = \frac{1}{2}k_L u^2 \tag{10}$$

where u is the displacement at the rod end.

One can separate the total displacement of the magnetostrictive driver into an active component and a passive component. The active component is the free displacement of the driver, $u_H = d_{33}HL$. The passive component is the elastic response u_{el}, which opposes u_H as a result of the transducer doing work against an external load (possibly including work against a prestress mechanism). The net displacement is $u = u_H - u_{el}$ (59). The tip of the driver is subjected to a total force F, where the passive displacement is $u_{el} = F/k_T$ and the total tip displacement is

$$u = u_H - \frac{F}{k_T} \tag{11}$$

For a linearly elastic external load, the force acting upon the driver end is $F = k_L u$. Substitution of this expression into equation 11 yields

$$u = u_H - \frac{k_L u}{k_T} \tag{12}$$

or, equivalently, after defining $t = k_L/k_T$

$$u = \frac{u_H}{1+t} \tag{13}$$

Finally, substitution of equation 13 into equation 10 and letting $k_L = t\ k_T$ yields

$$E_M = \frac{t}{(1+t)^2}\left(\frac{1}{2}k_T u_H^2\right) \tag{14}$$

Defining $E_0 = k_T u_H^2/2$ as the intrinsic energy of the magnetostrictive driver, E_M/E_0 is plotted in Figure 7 as a function of t, where it is apparent that the energy is maximum for $t = 1$. This situation indicates that stiffness matching is desired to achieve maximum output energy. It is emphasized that in some prestress mechanism designs, a spring or a set of washers is placed in series with the magnetostrictive driver. The spring stiffness has to be accounted for in calculations of stiffness matching. As noted previously, the driver stiffness is directly related to the elastic modulus E_y^H, which can be measured in different ways (50,52).

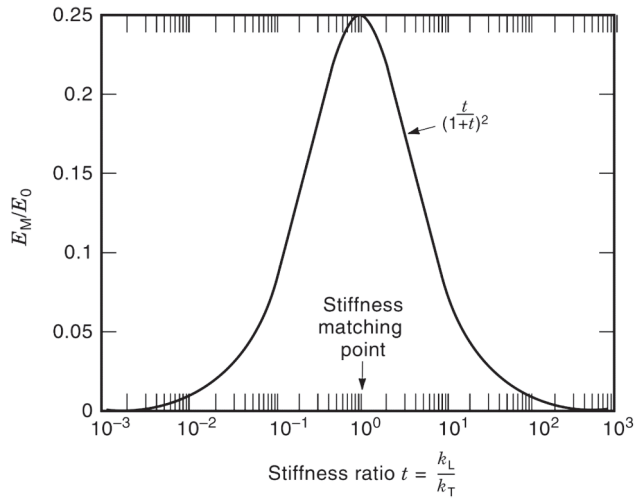

Figure 7. Normalized mechanical energy output is maximized for stiffness matching between the magnetostrictive driver and the combined transducer and external load stiffness characteristics (59).

Actuator Power Limitations. As discussed in References 60 and 61, the power output near resonance may be stress or field limited, depending on whether the mechanical quality factor Q is greater or smaller than the optimum value. This optimum Q hovers around unity for Terfenol-D (46). Hence, a low Q raises the maximum power limit of the transducer near resonance. In addition to the ability to handle more power, a low Q means a broader operational bandwidth. This situation may or may not be desirable because at low Q, the transducer is less able to filter out unwanted modes of vibration that might lead to harmonic distortion. This highlights some of the compromises present in designing a transducer's mechanical quality factor. Figure 8a depicts a typical radiated power limit Q curve indicating typical performance trade-offs at frequencies near transducer resonance for a Terfenol-D transducer, and Figure 8b shows an equivalent circuit representation of the transducer based on linear behavior.

Figures of Merit. The single-most important transducer FOM is the magnetomechanical coupling factor k (eq. 2) (57). This is particularly true in the low-signal linear regime, where k^2 quantifies the fraction of magnetic energy that can be converted to mechanical energy per cycle, and vice versa. Improvements in manufacturing techniques have helped increase the magnetomechanical coupling factors reported in bulk Terfenol-D. Values of $k \approx 0.7$ are commonly reported for Terfenol-D ($k \approx 0.3$ for

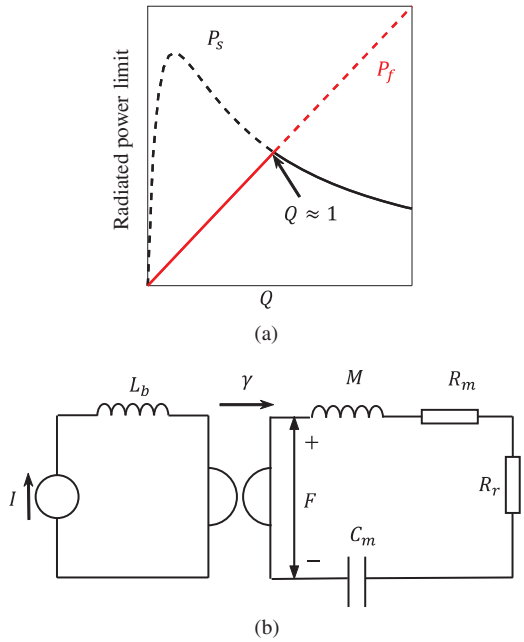

Figure 8. (a) Radiated power versus quality factor Q shown as the minimum of the stress-limited output P_s and the field limited output P_f. (b) Van Dyke transducer equivalent circuit representation for the magnetostrictive device used to predict (a), where I = current, L_b = blocked inductance, γ = gyrator ratio, C_m = open-circuit compliance, F = force, M = mass, R_m = mechanical resistance, and R_r = radiation resistance (60).

nickel), while recent studies report a value of $k = 0.75$ for Galfenol (49). A transducer's coupling factor will be lower than that of its magnetostrictive core due to magnetic, mechanical, and thermal losses inherent to other aspects of the device design and its components.

Under ideal lossless conditions, the resonance and antiresonance frequencies of the electrical impedance function in Figure 9a–c represents f_r and f_a as defined by the mobility impedance. In Figure 9b, the prestress is constant at 1.0 ksi (kilopound per square inch) and in Figure 9c the magnetic field is constant at 75 Oe. In the presence of losses, f_r and f_a shift slightly from the resonance and antiresonance points. Based on electroacoustic principles (3), it can be demonstrated that k is directly related to the system resonant and antiresonant frequencies, f_r and f_a. Assuming no losses,

$$k^2 = 1 - \left(\frac{f_r}{f_a}\right)^2 \tag{15}$$

The k dependence on AC field intensity and magnetic bias condition is clearly demonstrated in References 50 and 62. In a lossy magnetic circuit, however, this relationship is somewhat different, although the essential aspects are preserved (51). The effect of losses can be minimized by carefully designing the magnetic path and by using laminated material for the driver and all components of the magnetic circuit flux path by using either radial or longitudinal slots as appropriate. The penalty is typically increased complexity in manufacture and modeling.

Transducers intended for underwater use are often rated according to the desired characteristics of these devices: high power P, low resonant frequency f_0, low mass M (or volume V), and low quality factor Q. Hence, the definition FOM = PQf_0V is commonly found in the literature. Claeyssen et al. (63) presented a comparison of several Terfenol-D and PZT devices with FOM ranging between 10 and 655 J/m^3, where a Terfenol-D flextensional has a remarkable 655 J/m^3 figure of merit. A similar PZT device reached only 15 J/m^3; the difference is caused exclusively by the much smaller strain output of the PZT since the acoustical power radiated is proportional to the strain squared (63).

5.2. Types of Devices

In order to illustrate the needs and issues of different applications, we classify magnetostrictive transducers into three broad categories:

1. *High-power, low-frequency applications:* These applications are typically associated with underwater acoustic generation and communications. The designs discussed here are the flextensional transducer, the piston-type transducer, and the ring-type transducer.
2. *Motion generation:* In this category, we include transducers designed to do work against external structural loads. The motion may be linear, such as in the inchworm or Kiesewetter motors, rotational, or bending.
3. *Ultrasonic applications:* This category involves a fairly broad range of actuators ranging from surgical applications to ultrasonic joining.

Despite the differences among the three categories, there is intrinsic commonality to all magnetostrictive devices based upon the magnetomechanical nature of the device. First of all, it is often desirable to achieve linearity in the performance. Because magnetostrictive materials respond nonlinearly to applied magnetic fields (hysteresis, quadratic response at low field, saturation at high fields), it is common practice to subject the material to mechanical and magnetic bias (known as bias conditions). A magnetic bias is supplied with permanent magnets, located in series or parallel with the drive motor, and/or with DC currents. The mechanical bias is applied by structural compression of the driver with either bolts or via the transducer structure itself, such as in flextensional transducers.

Second, maximum effectiveness is obtained at mechanical resonance, where dynamic strains of peak-to-peak amplitudes higher than the static saturation magnetostrain can be achieved. Dynamic strains are of primary importance in low-frequency, high-power transducers, namely, those for sonar and underwater communications.

Among the other technological issues that affect the design and operation of magnetostrictive transducers are thermal effects, transducer directionality (determined by ratio between size and acoustic wavelength), resonant operation, and power source.

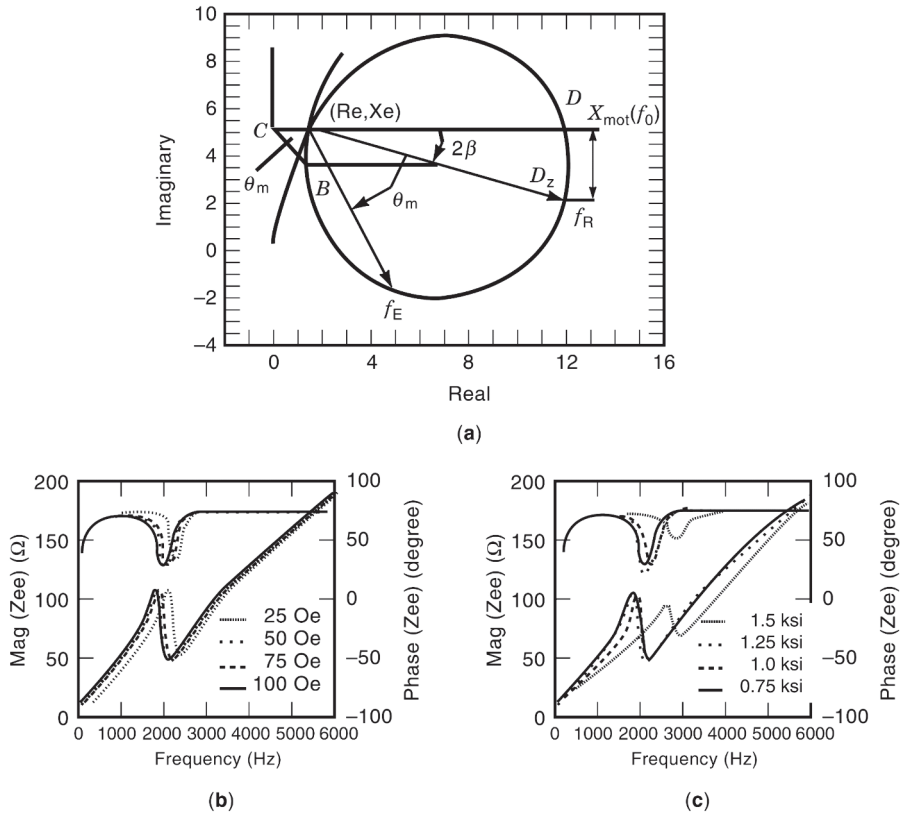

Figure 9. Measured Terfenol-D transducer electrical impedance functions. (a) Nyquist representation indicating diameter of mobility loop for use in determination of f_r. (b) Impedance for 1.0 ksi prestress at varied AC drive levels. (c) Impedance functions for 25 Oe drive level at varied initial prestress settings (62).

5.3. Low-Frequency Sonar Applications

Efforts to develop smaller sonar transducer systems capable of delivering increasingly higher acoustic power output have existed since the inception of sonar technology. Terfenol-D has proven attractive for underwater sound projection given its output strain, force, and impedance-matching characteristics. Not surprisingly, much of the research effort on magnetostrictive underwater devices has been performed by the US Navy, where Terfenol-D was originally developed.

The quest for more powerful sonar units forced researchers to increase either the size of the radiating surface or the vibration amplitude of the device. As a consequence, the former issue brought the re-emergence of a transducer principle first developed in the 1930s, the flextensional transducer. Magnetostrictive flextensional transducers offer high power at low frequencies. The power output of Terfenol-D flextensionals is about 25 times larger than that of PZT flextensionals because the dynamic strains are approximately 5 times larger and the power output is approximately proportional to the square of the strain (63). By comparison with the Tonpilz transducer, flextensionals present the advantages of providing a larger radiating surface per volume, using less active material, and requiring lower voltages. Technological challenges inherent to flextensionals are stress-induced fatigue, hydrostatic compensation, and prestressing for use in deep submersion. The Tonpilz-type transducer typically packs high power in a compact size. Moreover, because these transducers use an oversized piston for acoustic field generation, the diameter of the active element and magnetic circuit components can be increased without change in overall transducer diameter. A variation of the Tonpilz design is that with two-end radiating surfaces, which have an impact on the radiated acoustic field's directivity pattern. Square-ring transducers are used in either omnidirectional or directional mode. They provide low-frequency acoustic emissions.

A discussion of actuator devices for sonar applications is presented next. The discussion addresses the three main types of devices: the flextensional, the ring-type, and the piston-type.

Flextensional Actuators. Flextensional transducers radiate acoustic energy by flexing a shell, usually oval-shaped, caused by the longitudinal extension and contraction of a cylindrical drive motor mounted in compression inside the shell. These transducers are capable of producing high power at fairly low frequencies. Their history dates back to 1929 – 1936, when the first flextensional device for use as a foghorn was first built and patented by Hayes at the NRL (64).

Several factors limited the effectiveness of the early flextensional devices. Hayes's original design lacked a preload mechanism, which limited the strain and force

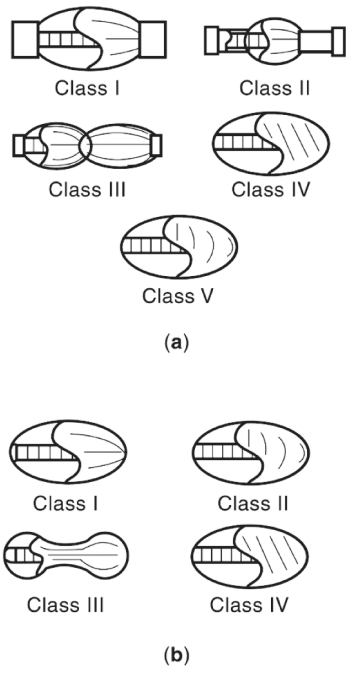

Figure 10. (a) Brigham and Royster classification scheme for flextensional transducers (66,67). (b) Pagliarini and White classification scheme for flextensional transducers (71–73).

capability of the transducer and lead to fatigue-related failure. The parallel development in the late 1920s of the ring transducer, a relatively cheaper and more rugged device with similar electroacoustic efficiency, severely undermined the budget destined for research on flextensionals. The flextensional concept was a high-power, high-efficiency transducer being used in the wrong field. It was not until the 1950s that flextensionals started to be considered for underwater applications, leading to a 1966 patent by Toulis (65). This device was nearly identical to Hayes's, except for the explicit intention for underwater projection and the use of a piezoelectric stack for driving the device. Interestingly enough, the flextensional transducer is usually credited to Toulis (66).

Flextensional transducers are identified by class. There are two different classification schemes, as shown in Figure 10a and b and at least two proposed variations of those. The reader is pointed to the references for further details.

In the classification scheme of Brigham and Royster (66,67), the radiating surfaces of class I flextensionals are formed by revolving an ellipse around its long axis with the magnetostrictive driver mounted on compression inside, along the major axis. A variant of this design known as the University of Miami flextensional has flat surfaces as described in Reference 66. The class II flextensional is essentially a modified class I in which, in order to accommodate more active material, the major axis is extended in both directions. The extra amount of active material allows more power handling without changing the fundamental resonance of the oval radiator. One strong limitation of the flextensional design is the narrowband response. To overcome this limitation, a class III design has been proposed. The shell of the class III flextensional consists of two class I shells of slightly different sizes grated together. The two closely spaced resonances help to broaden the acoustic bandwidth beyond that of the class I design. The most common shell geometry is that of the class IV flextensional. Typically, the shell is convex in shape, although there are variants, such as the flat-oval shell or the concave shell of Merchant (classified type VII by Rynne) (68,69). Finally, the class V consists of two shallow spherical caps attached to either side of a vibrating ring or disk (sometimes called clam shell). This design is often credited to a 1959 Abbott patent (70), although this design had been described by Pallas in 1937 (44). The Abbott patent shows a ceramic-driven unit with either concave or convex spherical shells. Note that in the Brigham–Royster scheme, classes I, IV, and V are basically distinguished by shape. On the other hand, classes I, II, and III are differentiated by end use (i.e., class II is a high-power version of class I, and class III is a broadband version of class I).

The Pagliarini–White scheme classifies flextensionals in four classes (I–IV), based exclusively on shell geometry (71–73). Class I and class II are similar to Brigham–Royster's classes I and V. Class III is known as the barrel-stave flextensional, and class IV is the typical oval-shaped shell similar to Brigham–Royster's class IV. Jones (72) and Rynne (69) have presented their own classification schemes by subtly modifying the previous schemes.

It is characteristic of flextensional transducers to have two types of radiating modes: a low-frequency flexing mode or modes (74) associated with bending of the shell, and a higher frequency breathing mode, in which the whole shell expands and contracts in unison. As the name implies, the desired mode of vibration is a flexural one. However, the breathing mode is acoustically more like a monopole; thus, it is usually of higher efficiency and improves the effective system magnetomechanical coupling factor. This higher mode has a strong effect on the parameters used to describe the flexural modes. Under hydrostatic pressure, the shell geometry determines whether the flexing mode occurs in-phase or-out-of-phase with respect to the longitudinal vibration of the driver. The former case is characteristic of the class IV flextensional, whereas the latter case is characteristic of Merchant's barrel-stave design.

In the class IV design, the hydrostatic pressure acting on the shell tends to unload the magnetostrictive driver. This presents a technological challenge that defines the compromise between acoustic power and submersion depth. This problem has been addressed in different ways, including depth compensation, mechanical filtering, and change of the shell geometry to concave instead of convex (Merchant).

In summary, flextensional devices designed for use with magnetostrictive drivers offer several advantages over other transducer materials such as PZTs, but successful demonstrations of their practicality for actuation are fairly recent. One such work reports a Terfenol-D-powered acoustic projector operated at a depth of 122 m (400 ft) driven to a source level of 212 dB (Ref. 1 μPa at 1 m) (5). It has been shown (46,63) that good magnetomechanical coupling and efficiency characteristics are possible in flextensional devices. Design considerations such as magnetic circuit design, unloading of the magnetostrictive driver

caused by submersion depths, effects of cavitation at shallow depths, and stress-induced fatigue in the shell have been studied in detail (5).

Piston-Type Actuators. High dynamic strains are instrumental in achieving high acoustic power radiation. As with many other transducer designs, the availability of giant magnetostrictive materials such as Terfenol-D makes it possible to design more powerful underwater piston transducers with little or no bulk penalty. It has been suggested (63) that because of the need for much less active material, the cost of a Terfenol-D-driven piston transducer would be lower than, for instance, that of an equivalently rated piezoelectric flextensional transducer. The simpler design and the lack of bending parts likely to suffer fatigue-induced failure also indicate some of the advantages of piston-type designs over conventional flextensional transducers. The Tonpilz transducer (Tonpilz is German for "sound mushroom") is simple in principle, as illustrated in Figure 11a. The magnetostrictive rod is surrounded by a drive solenoid, which provides the magnetic field excitation. The magnetostrictive element actuates upon an inertial mass ("tail" mass) and has a front radiating surface that generates the desired sound waves. The magnetic path is completed by magnetic couplers and a magnetic return path cylinder. In fact, the magnetic circuit can have many possible configurations. For instance, some designs use cylindrical permanent magnets and ferromagnetic end pieces known as a "barrel magnet" configuration instead of the "stacked magnet" configuration shown in Figure 11a. Each configuration has a specific set of merits, which means that the optimum magnetic circuit configuration should be identified based upon the particular application requirements (75). As a rule of thumb, rods shorter than 20 cm and with diameters under 2.5 cm produce higher magnetic coupling, on the order of 5%, when employed in a barrel magnet configuration over a stacked magnet configuration. However, when longer and thicker rods are used, saturation and end effects are more likely to occur in the barrel magnet configuration. The stacked magnet configuration does have the potential for significantly increasing the systems' resonant frequency due to stiff pole magnets located in series with the magnetostrictive element. Typical permanent magnet materials currently in use are Alnico V, samarium–cobalt, and neodymium–iron–boron, while the magnetic return materials currently used are laminated steel and ferrites.

Magnetostrictive Tonpilz radiators have been shown to produce high source level outputs and very high FOMs. Steel (76) described a Tonpilz transducer in which six hexagonal cylinders of Terfenol-D are arrayed forming a tube inside which there is a prestress rod. The transducer itself is mounted on its central node in such a way that the magnetostrictive tube and the head mass form a so-called balanced piston design. The vibration of head and tail masses is almost symmetrical (with the same velocity but in opposite directions). The advantage of this design is that the Terfenol-D tube is isolated from hydrostatic pressure and freed of undesirable shifts in resonant frequency as a result of changing preloads. However, balanced piston operation occurs only near resonance, so the device is a narrow bandwidth transducer.

Hybrid magnetostrictive/piezoelectric transducers designed at the NUWC (Naval Underwater Warfare Center) (77) are capable of broadband operation by virtue of its double resonance configuration. The transducer consists of a series arrangement of a tail mass, an active driver, a center mass, a second active driver, and a head mass. Because the velocities of the piezoelectric and magnetostrictive drivers are 90° out of phase with each other, self-tuning similar to that in the balanced piston design is obtained. In addition, the improved coupling coefficient of this device translates into better acoustic response at even lower frequencies than in conventional Tonpilz transducers of similar size and weight.

Meeks and Timme (78) presented a Tonpilz vibrator consisting of three Terfenol-D rods spaced 120° apart, head and tail masses, and a center rod for mechanical and magnetic biasing. The transducer was not as powerful as more recent units, but it was useful for demonstration of the potential of Terfenol-D for this type of application.

Claeyssen and Boucher (79) developed a set of magnetostrictive transducers capable of very high acoustic power output. An initial design, called the quadripode, uses four rods to vibrate the radiating piston at an in-water resonant frequency of 1200 Hz. A follow-up design, named quadripode II, has better effective coupling and broader operational bandwidth, thanks to modifications in the head mass and prestress rod. Both transducers feature a forced cooling device. A transducer based on three rods instead of four, called Tripode, was also developed that produces twice the power output as the four-rod transducers (3.8 versus 1.6 kW), packed in less than half the volume (2.2×10^4 cm^3 versus 5.1×10^4 cm^3). Hydrostatic compensation permits deep submersion up to 300 m. The source level of the Tripode device at resonance (1.2 kHz) is 209 dB (Ref. 1 μPa at 1 m), and the FOM is 24 J/m^3 (63). Another design is the double-ended vibrator; a radiating piston replaces the tail mass so that the transducer is symmetric around its midpoint. This transducer competes favorably against the flextensional in the 300 Hz range because of its simpler, cheaper design, the lack of fatigue-related problems, and the lower voltages required for operation. More details on this device can be found in Reference 63 and 79.

Piston-type magnetostrictive transducers genearate limited strokes. Chakrabarti and Dapino (80,81) implemented a compact and simple displacement amplifier that operates on the principle of fluid amplification. This design was demonstrated for vehicle mount actuators, achieving a 2 mm stroke up to 200 Hz, but it is applicable to high-power sonar.

Ring Actuators . Ring transducers employ the radial vibrations of tubes or plates. This concept was first developed in the late 1920s (44). The interest in ring transducers during those early days was based on the ruggedness and lower cost compared to other available transducer technologies. One example of those early magnetostrictive devices is the radially vibrating cylinder patented by Hayes in 1935 (82).

The ring transducer concept was extensively researched, not only with magnetostrictive materials as the

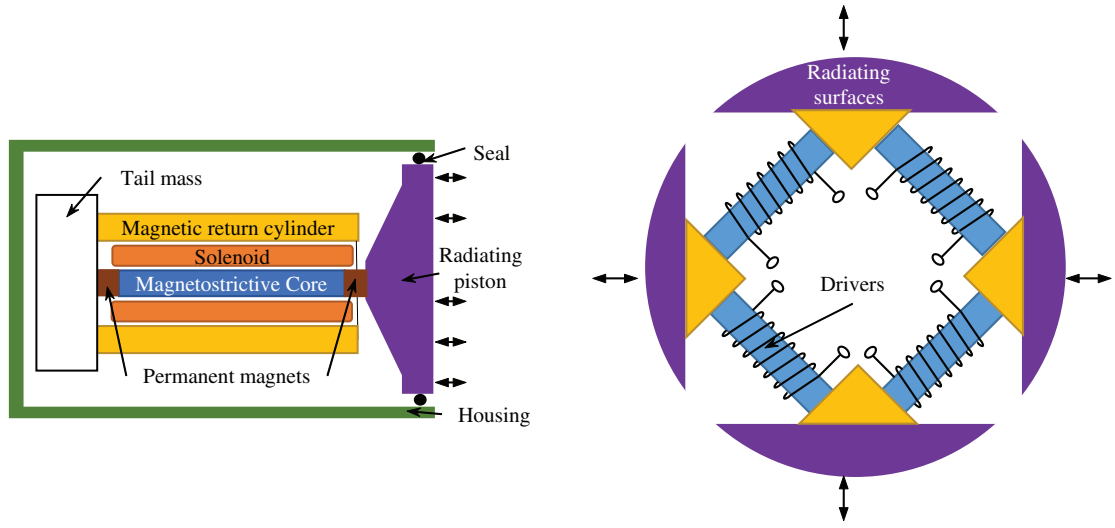

Figure 11. Typical magnetostrictive transducers. (a) Tonpilz actuator. (b) Ring actuator.

active driver but also with piezoelectric ceramics (83). Today, the better coupling factor and lower elastic modulus of the rare earth–iron alloys gives these materials an edge over conventional piezoelectrics.

For instance, the square ring transducer (84) can generate either omnidirectional or directional sound propagation at low frequencies. Four Terfenol-D rods are arranged forming a square; the radiating surface consists of four curved pistons attached to each corner of the square, as shown in Figure 11b. A similar principle was utilized in the octagonal ring transducer discussed in Reference 85. The dipole mode is accomplished by switching the magnetic bias on two of the rods and maintaining a constant direction of the AC magnetic field on all four rods. This feature translates into a transducer having two effective resonant frequencies and Q values, one for each mode of operation.

5.4. Motion/Force Generation Devices

There is growing interest in the use of magnetostrictive devices as a source for motion and/or structural forces. A variety of magnetostrictive motors have been designed, with the objective of providing accurate actuation at a given force rating over a range of operating frequencies. Conventional electromagnetic and hydraulic devices are commonly used in combination with gear boxes for motion conversion, and as a result are prone to mechanical play and bulkiness. Magnetostrictive motors produce outputs comparable to many conventional systems without the need for a gearbox interface, thereby avoiding many of the added system design issues (mass, volume, wear, play, backlash, etc.).

In this section we classify magnetostrictive motors as linear rotational, or bending depending on the type of motion provided by the device.

Linear Motors. The simplest type of linear motion device, a piston actuator, was presented in Figure 1. Piston devices output mechanical strains and forces over bandwidths from DC to over 5 kHz. Piston actuators have been employed in a variety of applications, ranging from linear positioners and control of valves to achieving active vibration control in structures in single-ended configurations (86–89) and as active struts in double-ended configurations (90). The stroke of these devices is limited to the strain of the magnetostrictive driver element. The stroke can be increased by going to a longer device or using any of a variety of simple motion amplification devices, with the drawback of introducing play.

Magnetostrictive motors capable of displacement strokes greater than the core saturation strain include the elastic wave motor (EWM), or Kiesewetter motor (91). The EWM consists of a cylindrical Terfenol-D rod moving in inchworm-like fashion inside a stator tube (Figure 12). The magnetostrictive core is snugly placed inside the stator tube; the stator is in turn surrounded by several short coils located along its length. As the first coil is energized, the magnetostrictive element lengthens locally, while its diameter decreases by virtue of the volume invariance of the magnetostrictive effect. When the field is removed, the rod clamps itself again inside the tube. By energizing the coils sequentially along the length of the stator, it is possible to induce a displacement d per cycling of the coils as indicated in Figure 12. The step d can be adjusted by varying the magnetic field intensity generated by the coils. The speed of the motor is regulated by the speed at which the coils are energized and by the shielding effects of eddy currents. Normally, the coils are excited with a single traveling pulse, but increased speed can be achieved by multiple-pulse excitation. Reversal of the direction of motion is achieved by reversing either the bias polarization or the direction of the traveling pulse. The device load handling rating is constrained by either the interference forces generated between the core and the stator tube or the blocked force capability associated with core elongation. A prototype designed for use in the paper industry develops 1000 N of force, 200 mm of stroke, and 20 mm/s

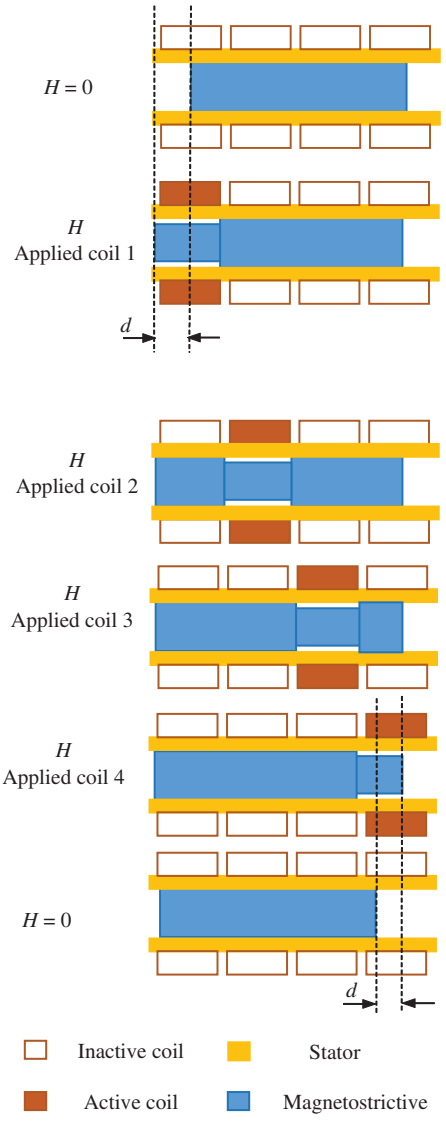

Figure 12. Principle of operation of the Kiesewetter inchworm motor. Energized solenoids are marked in black; passive solenoids are white.

speeds (92). Other areas of application for this device are valve control and precision positioners. The EWM has also been utilized for active control of the profile of aircraft wings. The proof-of-concept device in Reference 93 facilitates fuel savings in aircrafts of 3–6%, by changing the profile of the "smart trailing edge" at speeds of 0.4 mm/s and strokes of 25.4 mm.

A variant of the inchworm principle uses fixed-position and translating transducer elements to simultaneously clamp and unclamp adjacent sections of a load shaft (Figure 13). When the translating clamps are engaged, pusher transducers are actuated to move the translating clamps from their resting position. When the fixed position clamps are engaged, the pusher elements return the (now unclamped) translating elements to their resting position. The fixed position clamps maintain the load shaft position during the return portion of the translating clamps' motion cycle. By sequential clamping and unclamping, bidirectional linear motion of the load shaft is induced as illustrated in Figure 13. The device load handling rating is constrained by either the clamping forces generated between the load shaft and clamping transducer elements or by the blocked force capability associated with the pusher transducers.

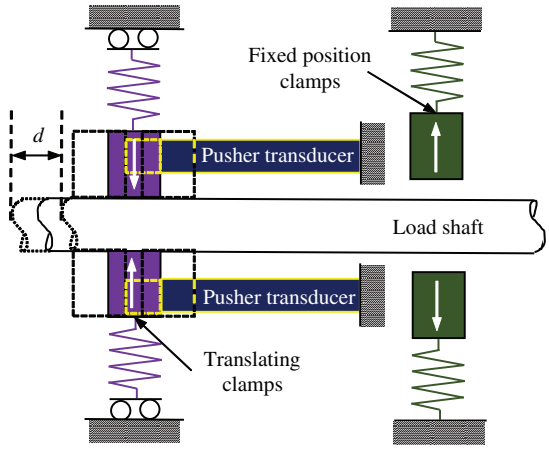

Figure 13. Principle of operation of the discrete inchworm actuator.

The design of Figure 13 is often implemented utilizing piezoelectric clamps and magnetostrictive pusher transducers, or vice versa. The resulting hybrid device presents a resonant RCL load to the supply amplifier(s). The reduced reactive power load helps to simplify the amplifier design. The 180° phase lag between the piezoelectric stacks and the 90° phase lag between the inductor current and the capacitor voltage provide natural timing for the clamping, unclamping, and linear motion actions. A prototype (95) achieves a stall load of 115 N and no-load speeds of 25.4 mm/s. A similar idea (96) uses a magnetostrictive bar as a load shaft, allowing a very compact design. When used in conjunction with a dedicated switching power drive, the predicted speed of the motor is 7.8 mm/s at a frequency of 650 Hz and force of 130 N. Other examples of linear magnetostrictive motors are the push–ends of the slider rapidly shrink towardspull actuator by Kvarnsjo and Engdahl (97), the oscillating level actuator by Cedell et al. (24), and the broadband shaker by Hall (41).

Zhang et al.(94) proposed a new driving strategy for microrobotics that achieves long stroke and fine positioning resolution without implementing large numbers of coils or complicated clamping mechanisms (Figure 14). The interplay of inertia and frictional forces propels the slider along the stator pipe, as shown in Figure 15. A sawtooth wave current energizes the coils wound around the Galfenol element. As the driving current slowly increases, the friction force between the stator pipe and the slider dominates; the right mover slowly elongates while the frictional part remains clamped. When the driving current is abruptly shut down, the inertia of the slider dominates, such that both ends of the slider rapidly shrink toward the center (slippage effect). Continuous movement is achieved by repeating this operation, and inverse movement can be achieved by changing the current direction. This linear

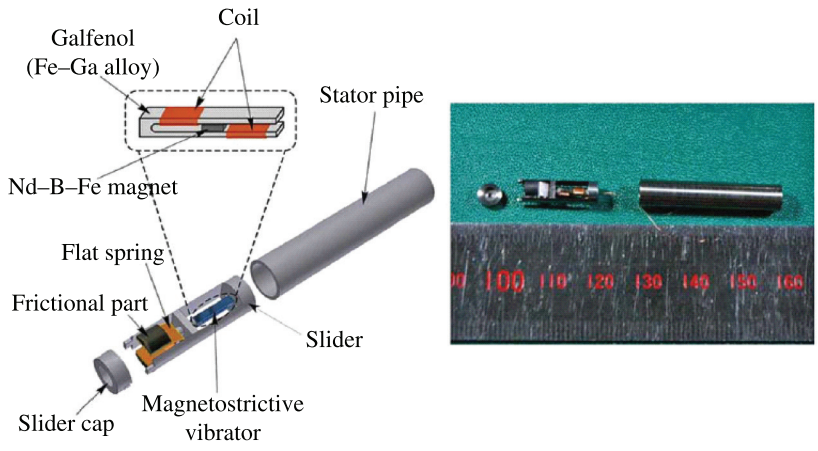

Figure 14. Configuration of Galfenol linear motor for microrobots. (Reprinted with permission from Reference 94. Copyright 2009, Elsevier.)

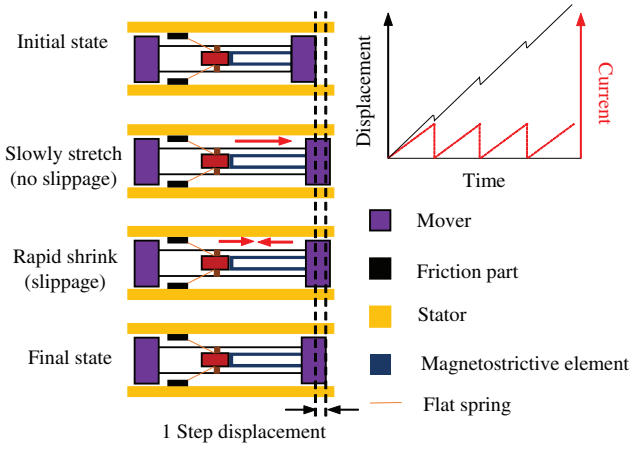

Figure 15. Schematic structure and propelling principle of linear Galfenol motor.

motor achieves a maximum speed of 0.56 mm/s for a 1 kHz, 0.15 A sawtooth driving current (94).

Rotational Motors. The magnetostrictive principle has been employed in rotational motors as well. Several areas such as the aerospace and automotive industries benefit from the higher controllability of the "smart material" motors compared to conventional hydraulic or electromagnetic devices. In particular, there is a need for high-torque, low-speed motors, in which the inchworm technique is particularly suitable. A device having these characteristics, capable of a maximum torque of 3 N · m and speed of 3°/s, was presented by Akutsu (98). An inchworm prototype was presented by Vranish et al. (99), a design capable of very high torque of 12 N · m at speeds of 0.5 rpm and precision microsteps of 800 μrad. Despite the great positioning accuracy and high holding torques, to date the inchworm-type devices sometimes lack in efficiency. To overcome this, a resonant rotational motor based on a multimode stator has been proposed by Claeyssen et al. (100). Two linear Terfenol-D actuators are used to induce elliptic vibrations on a circular ring (stator), which in turn transmits rotational motion to two rotors pressed against the ring (Figure 16). The prototype did not achieve the expected deficiencies, but at 2 N · m of torque and speeds of 100°/s, the potential of this idea has been demonstrated.

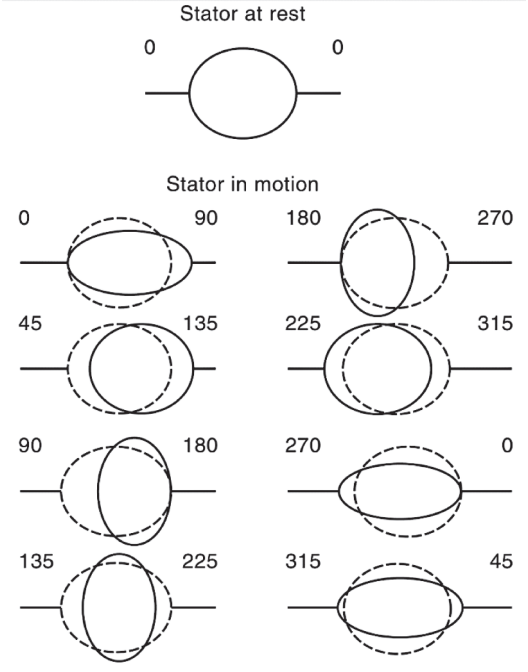

Figure 16. Modes of vibration of the rotational motor of Cleayssen et al. (100).

Ueno et al. (101) proposed a new Galfenol-based miniature motor, as shown in Figure 17, consisting of four square Galfenol rods with wound coils, a permanent magnet, and a spherical rotor (iron ball). The permanent magnet located in the center is used to provide a DC bias magnetic field and to hold the rotor to the edges of the rods. The principle of the rotational movement is similar to the linear micromotor illustrated in Figure 15. Two sawtooth currents with a 180° phase difference are applied to a pair of opposing coils (see in Figure 17b). As the driving current slowly

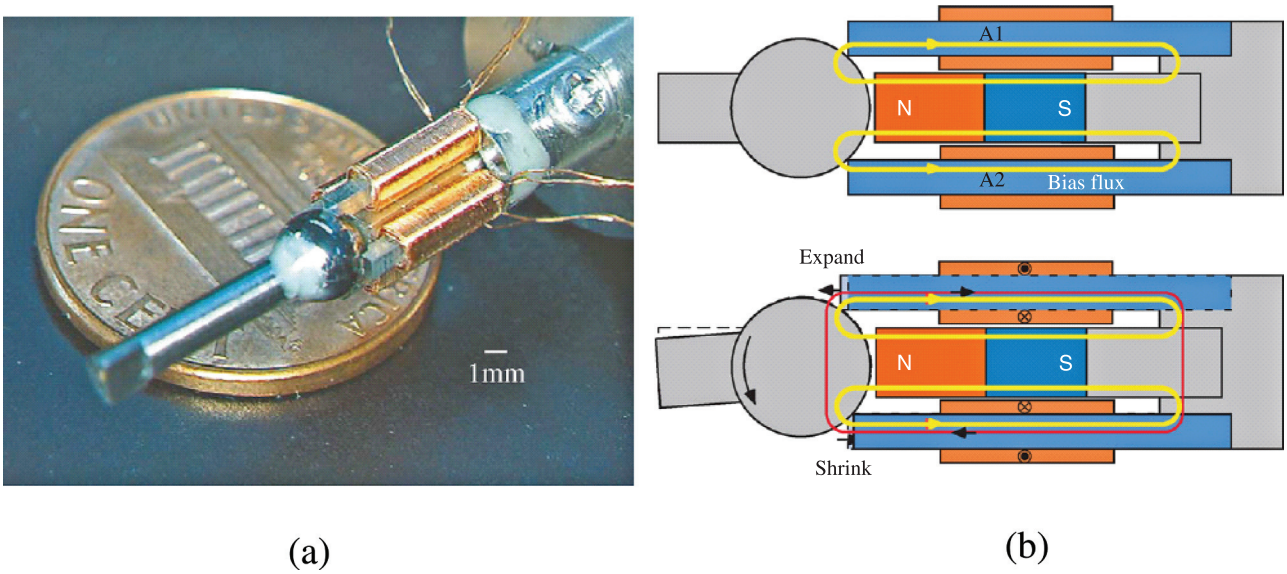

Figure 17. (a) Miniature spherical motor (101). (b) Magnetic flux path and rotor positions at no driving current (top), and current of 180° flowing to opposing coils (bottom). (Reprinted with permission from Reference 94. Copyright 2009, Elsevier.)

increases, the top coil generates a magnetic field acting along with the dc bias, and thus the Galfenol rod on the top expands. The Galfenol on the bottom reciprocally shrinks, since the coil-induced magnetic field acts against the DC bias. The friction force rotates the rotor counter clockwise. When the driving current suddenly drops to 0, both rods rapidly return to their original shapes, but the rotor stays in position due to the slippage effect between the iron ball and the rods. Similarly, the rotor can rotate into or out of plane by controlling the other pair of opposing coils. This rotational motor with two degrees of freedom is able to generate an angular velocity of 35°/s and a maximum torque of 0.2 mN m.

A proof-of-concept hybrid magnetostrictive/piezoelectric rotational motor is illustrated in Figure 18 (102). A piezoelectric stack clamps a piece of friction material onto the rotating disk, while two magnetostrictive rods move the clamp tangentially to the disk to achieve rotational motion. The direction of induced motion is bidirectional, determined by the direction of excitation of the oppositely connected driving solenoids. Once again, the inductive and capacitive nature of the transducer's electrical impedance is used to minimize the reactive power requirement on the power amplifiers, and the timing is naturally determined by the time lag between inductors and capacitors. Thus, operation near electrical resonance is ultimately desired. This design has been shown to achieve near 4 rpm at excitation frequencies between 650 and 750 Hz and voltages between 30 and 40 V.

Bending Actuators. Because Terfenol-D is brittle and can bear little tensile or torsional load, the material has been embedded into flexible matrices to enable bending actuators (103). A disadvantage of this approach is that magnetomechanical coupling property differs from the monolithic layer and depends heavily on the prestress and

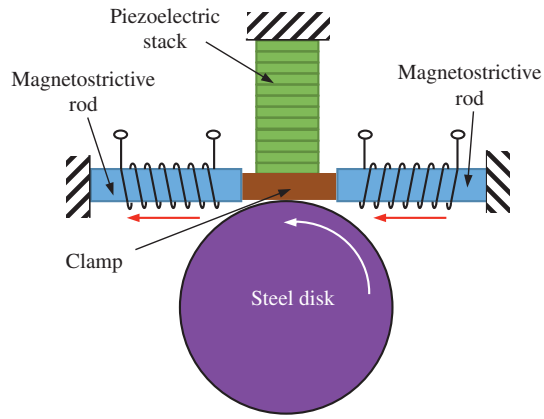

Figure 18. Hybrid piezoelectric and magnetostrictive rotational motor (102).

particle orientations in the resin, which are difficult to measure. Galfenol has high mechanical strength, and thus can be directly machined as beams or sheets that tolerate significant tensile and shear stresses. Shu et al. (104) and Chakrabarti and Dapino (105) developed a unimorph beam structure that consists of a thin active Galfenol layer bonded to a passive nonmagnetic stainless steel layer. The Galfenol layer (polycrystalline $Fe_{81.6}Ga_{18.4}$) tends to elongate along the magnetic field direction, while the passive layer (nonmagnetic 316 stainless steel) restricts the deformation of the Galfenol layer, thus inducing bending of the tip. Both the resin with sparse Terfenol-D particles and the Galfenol sheet can be bonded to structures to actively compensate for structural vibration (106).

5.5. Ultrasonic Devices

Ultrasonics is the science of acoustic waves with frequency above the human audible range, nominally above about 20 kHz. This definition is somewhat arbitrary, since most

sound propagation phenomena behave the same at sonic and ultrasonic frequencies. However, the distinct features of ultrasonic devices merit a separate study from other types of transducers. For instance, a challenge in the generation of airborne ultrasound is the difficulty associated with coupling the energy generated by the electroacoustic device into the medium due to the large impedance ratio mismatches between the transducer and the medium (on the order of 10^{-5}). At very high frequencies in the megahertz range, ultrasonic energy can be concentrated by shaping a thin-film transducer into a bowl shape. The center of curvature represents the energy focus. An alternative way, usually employed at frequencies in the tens of kilohertz range, is by using a half-wavelength metal horn (the length of the horn is one-half the wavelength of elastic waves at the transducer's resonant frequency). The tapered shape of the horn produces an increase in the displacement, velocity, and pressure amplitudes, as illustrated in Figure 19 (107). Note that each profile has its own modal characteristics, thus the right shape must be carefully chosen for a given application.

Traditionally, the most common magnetostrictive materials used for ultrasonic applications were pure nickel and iron–cobalt alloys, such as Permendur (49% iron, 49% cobalt, 2% vanadium). The magnetostrictive material is shaped so that good closure of the magnetic flux is achieved, and several laminates of the material are stacked together to minimize eddy current losses. The power losses due to eddy currents are proportional to the square of the operating frequency, so at ultrasonic regimes their significance is high. The material is as usual driven with solenoids. These transducers are normally operated at the half-wave fundamental frequency, which means there is a node in the center plane of the magnetostrictive element. This plane, where no motion is produced, is used as a mounting point for the transducer assembly. Alternatively, an elastic mount can be used as shown in Figure 20 (108).

Devices similar to that of Figure 20, with or without a coupling horn are being used in diverse applications such as cleaning of intricate or hard-to-reach parts, emulsification and homogenization of immiscible liquids, atomization of liquids or inks, particle agglomeration, degassing of liquids, catalysis of chemical reactions, machining, welding of plastics and metals, medical therapy and surgery, metal casting, dispersion of solids in liquids, and foam control (109–112). The underlying principle behind each of these processes can be related to cavitation effects, heat generation, mechanical effects, diffusion, stirring, and chemical effects. Of these effects, cavitation is perhaps the one that plays an integral role in most processes. As the sound wave propagates within the medium, individual particles are alternatively subjected to compression and refraction, although their relative positions do not change. For large sound wave amplitudes, the magnitude of the negative pressure in the rarefaction areas, associated with the low-pressure half-cycle of vibration of the transducer, produces micrometer-size gaseous cavities to be formed. These cavitation bubbles grow until an unstable state is reached during the high-pressure half-cycle of operation,

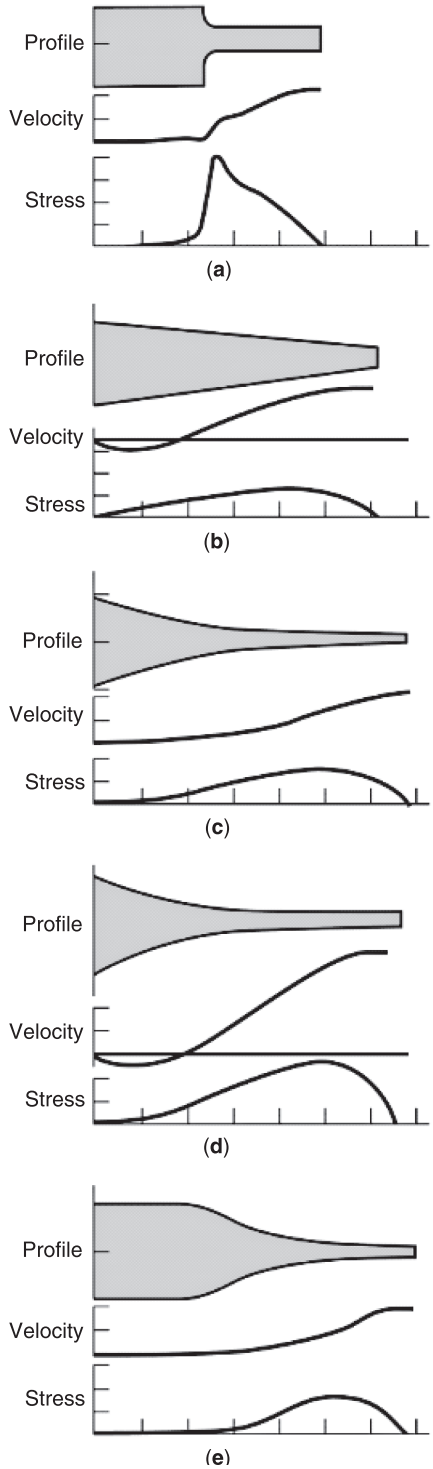

Figure 19. Geometry, velocity, and stress profiles of horns for amplifying the displacement output of ultrasonic transducers. (a) Stepped. (b) Conical. (c) Exponential. (d) Catenoidal. (e) Fourier (107). (Reproduced with permission, copyright © John Wiley & Sons.)

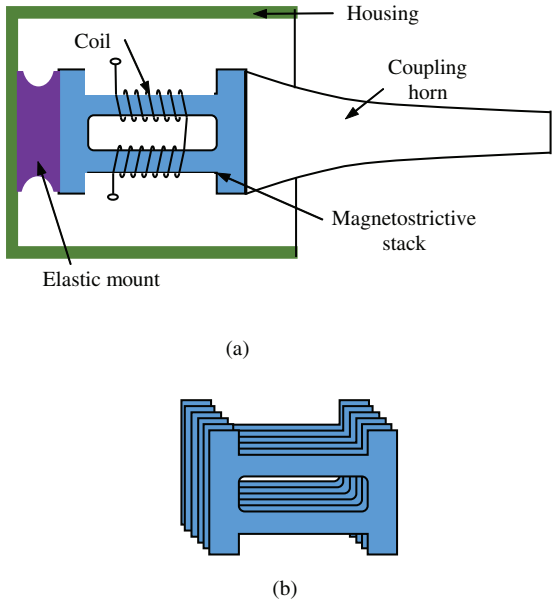

Figure 20. (a) Ultrasonic transducer with coupling exponential horn (108). (b) Laminates used to build a ultrasonic magnetostrictive stack.

in which the bubbles collapse giving rise to huge pressure gradients as the liquid rushing from opposite sides of the bubble collides. The implosion event generates a microjet that impinges at high velocity on the surface to be cleaned. It has been calculated that locally the pressure rises to about 10 ksi, with an accompanying temperature rise of about 10, 000 K (109). The combination of high speeds, pressure, and temperature, together with conventional cleaning agents, frees contaminants from their bonds with the surface.

Magnetostrictive transducers utilizing nickel as the active element are currently used for industrial cleaning and degassing of liquids, at operating frequencies of 20–50 kHz (Blue Wave Ultrasonics, PMR Systems, Pillar Power Sonics). For dental and jewelry applications, the operating frequencies exceed 50 kHz. Although piezoelectric transducers are sometimes preferred for megahertz-range ultrasonic generation, the ruggedness and durability of magnetostrictive devices constitutes a very desirable characteristic. In addition, magnetostrictive materials do not need to be repolarized when accidentally heated beyond the Curie point, as is the case with piezoelectrics.

Details on ultrasonic half- and quarter-wave prototype transducers using a GMPC (giant magnetostrictive powder composite) material can be found in Reference 24. The half-wavelength unit was tested for liquid atomization, whereas the quarter-wavelength unit was used for ultrasonic washing and, when coupled to a 10:1 horn, for welding of plastics and cutting of wood.

Both nickel and PZT materials are "high-Q" materials, that is, their characteristic response exhibits a sharp peak at resonance, providing a very narrow range of frequencies over which the material is capable of transducing large amounts of energy. The output and efficiency decrease drastically at operating frequencies away from the fundamental resonant frequency. This effect can prove very limiting in applications where the system resonance is prone to varying, such as due to load changes. On the other hand, Terfenol-D is a low-Q ($Q \leq 20$) material and hence it overcomes much of the bandwidth limitations of nickel and PZTs. Hansen reports (110) current progress in Terfenol-D-driven ultrasonic transducers for surgical applications (348 μm displacement at 1 MHz), and for degassing of liquids for the bottling industry. Ultrasonic welding and engraving using Terfenol-D are also being studied. A 15 kW, 20 kHz ultrasonic projector is currently being developed in an Etrema-NIST research effort (113). The projected areas of applicability of the device are devulcanization of rubber for recycling, catalysis of chemical reactions, and ultrasonic treatment of seeds to improve yield and germination efficiency.

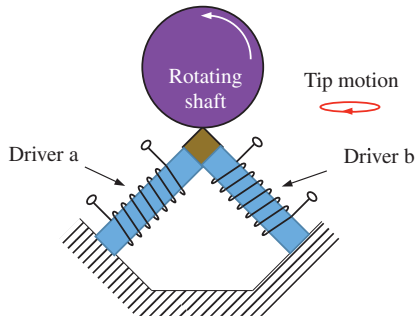

Figure 21. Terfenol-D ultrasonic rotational motor. (after Reference 98.)

Another field of high research and commercial interest is that of ultrasonic motors. The use of ultrasonic motors is being extensively explored in robotics, aerospace, automotive, and consumer applications. One visible example at the consumer level is the ring-type ultrasonic motor used for autofocusing camera lenses. Many kinds of ultrasonic motors have been developed, but two main categories can be distinguished (114): the vibrating driver type, and the progressive wave type. The vibrating driver uses the elliptical motion of a PZT driver, whereas the progressive wave motor uses the frictional force between the PZT driver and translator. Either type presents attractive features such as fine controllability, good efficiency, and compact size. However, the driving force is restricted by the friction generated between the moving surfaces, and most importantly, by the shearing strength of the PZT. To overcome these limitations, Akutsu (98) developed a rotational actuator using Terfenol-D to achieve large amplitude elliptical vibrations, high torque, and fine angular controllability. The motor, illustrated in Figure 21, has a speed of 13.1 rpm, and maximum torque of 0.29 N · m at a rotational speed of 1300 Hz.

It has been shown (115) that it is feasible to produce remotely powered and controlled standing wave ultrasonic motors (SWUMs) using thin-film rare earth–iron alloys. The motor is completely wireless, and the excitation coil can be placed away from the active rotor. This represents a unique feature, not possible to achieve with piezoelectric technology, which can be used for intrabody distribution of medication, micropositioning of optical components, and actuation of small systems such as valves,

electrical switches, and relays. A linear motor with these characteristics producing speeds of 10–20 mm/s and a rotational unit producing 1.6 μN· m of torque at 30 rpm were built.

5.6. Other Actuator Applications

A number of additional applications take advantage of the relatively large strains and force characteristics of magnetostrictive materials: wire bonding clamp for the semiconductor packaging industry (119); dexterous force reflection device for telemanipulation applications (120); hearing aid device based on the generation of low amplitude vibrations to bone, teeth, and similar hard tissue using Terfenol-D (121); magnetostrictive borehole seismic source (122); system for high-frequency, high-cycle fatigue testing of advanced materials using a magnetostrictive actuator (123); and magnetostrictive fuel injection valve (24). A review of additional actuators is given by Restorff (124).

In addition to position or force control, magnetostrictive actuators can be used to take advantage of the modulus change of these materials due to magnetic domain rotation, known as the Delta-E effect (125,126). Scheidler et al. (128) experimentally proved that the Young's modulus of Galfenol (polycrystalline $Fe_{81.6}Ga_{18.4}$) varies with respect to both applied magnetic field and stress. The Delta-E effect can be used in structural stiffness tuning and vibration isolation. Scheidler and Dapino (127) utilized ultrasonic additive manufacturing to embed a Galfenol sheet into a passive aluminum matrix. The bending stiffness of the Galfenol–aluminum composite can vary by 49% by controlling the magnetic field through the Galfenol sheet (127).

6. MAGNETOSTRICTIVE SENSOR APPLICATIONS

Magnetostrictive sensors rely on changes in magnetoelastic properties to convert the change in a physical parameter into an electrical signal that can be processed and transmitted. Position, torque, force, magnetic field, and other physical properties can be detected with these materials.

6.1. Sensing Effects

Magnetostrictive sensors can be divided into three groups based on how the magnetomechanical properties of the system components are used to measure the parameters of interest: (i) passive sensors, (ii) active sensors, and (iii) combined sensors. Passive sensors rely on the material's ability to change as a result of environmental stimuli to make measurements of interest. Passive sensors use the magnetomechanical effect such as the Villari effect to measure external load, force, pressure, vibration, and flow rates. Active sensors use an internal excitation of the magnetostrictive core to facilitate the measurement of core attributes that change in response to an external property. For example, the magnetic permeability of Terfenol-D is sensitive to temperature. With suitable calibration, temperature can be determined by measuring changes in the strain produced through excitation of a Terfenol-D sample with a known applied magnetic field.

Designs that employ two coils, one to excite the magnetostrictive component and one for measurement, are known as transformer-type sensors. The most common active sensors are the noncontact torque sensors. These sensors employ variations on a general theme of using a magnetostrictive wire, thin film, or ribbon wrapped around or near the specimen that is subject to a torque. The change in the magnetic induction can then be related to the torque acting on the specimen.

Finally, combined sensors that use Terfenol-D as an active element to excite or change another material have been developed. They will allow measurement of the property of interest. For example, a fiber optic magnetic field sensor uses the change in length of a magnetostrictive element in the presence of a magnetic field to change the optical path length of a fiber optic sensor. There are numerous examples of combined sensors, including those to measure current, shock (percussion) and stress, frost, proximity, and touch. Stress can be measured using photoelastic material, and highly accurate displacement measurements can be made with the help of a magnetostrictive guide. Fiber optics and diode lasers have been used with magnetostrictive elements to measure magnetic flux density (magnetometers) (122). Magnetostrictive sensors often require pickup coils to generate an electrical signal from magnetic flux density variation. Recent studies presented bonded laminated Terfenol-D to piezoelectric layers and created magnetoelectric materials that can directly convert stress in the magnetostrictive materials to electric signals (129). NDE (nondestructive evaluation) applications have also been developed, such as a corrosion sensor for surveying insulated pipes. Applications are discussed later in terms of the measured property or quantity: torque, magnetic field, damage/corrosion, motion, force, and miscellaneous characteristics.

6.2. Torque Sensors

Torque measurement is needed in a variety of applications and industries, including the automotive industry and high-speed machining. Magnetostrictive torque sensors are traditionally based on the inverse magnetostrictive effect (Villari effect), where a torque-induced change in stress in the target causes a change in the magnetization of a magnetostrictive element in the sensor–target system. This change in magnetization can be measured directly (passive) or as a change in permeability with active excitation (active). A thorough overview of torque sensor technology, focusing on magnetostrictive torque sensors, is given in Reference 130.

Noncontact Torque Sensors. A practical torque sensor configuration is the noncontact torque sensor. The change in stress in a ferromagnetic shaft is measured by detecting the change in permeability of a ferromagnetic element flux linked to the shaft. Figure 22 shows the basic design components, which include a C-shaped ferromagnetic core with an excitation coil and a detection coil. Two variables in the sensor system are the excitation coil current

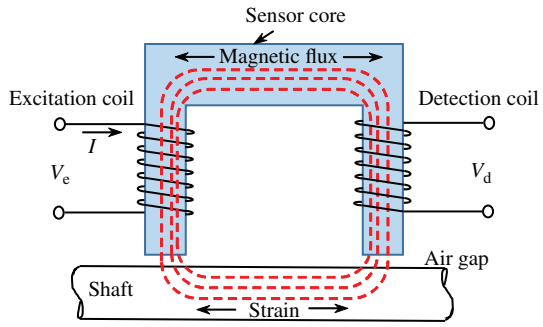

Figure 22. Noncontact torque sensor with excitation and detection coils around the legs of a C-shaped ferromagnetic core (54).

I and the air gap between the shaft target and the sensor core. Noncontact torque sensors are advantageous because implementation is simple and fast. The system is stable, accurate, and sensitive. Fleming studied various properties of these sensors, including nonlinearities caused by sensor element properties, the effects of magnetic saturation, and excitation frequency (131).

Thin-Film Torque Sensors. An alternative torque sensor configuration is to apply the magnetostrictive material directly to the target. This idea was developed by Yamasaki, Mohri, and their collaborators, who used a wire explosion spraying technique to adhere thin layers of Ni, Fe–Ni, and Fe–Co–Ni to shafts (132). In this method, the conductive wire is exploded at a high temperature into fine particles that adhere strongly to the shaft. The wire explosion technique results in a sufficiently strong adhesion, which they report increased sensor reliability relative to competing technologies that rely on epoxies to fix magnetostrictive material to a surface. When the shaft is twisted, stress in the film causes a change in its magnetization-applied magnetic field hysteresis loop. When two such regions of magnetostrictive material are surrounded by coils connected in a multivibrator bridge circuit (133) a change in voltage caused by a change in the torque can be detected. A linear, nonhysteretic relationship between the bridge circuit output voltage and the torque was obtained, with Ni and Fe_{42}–Ni_{58} providing the greatest sensitivity.

A second system using a 300 μm thick Ni layer applied by plasma jet spraying was investigated by Sasada et al. (134). The instantaneous torque on a rotating shaft was related to the magnetic circuit permeability measured using a pair of U-shaped magnetic heads positioned at ±45° from the shaft axis. The sensitivity of the measurements to the air gap between the shaft and the magnetic heads was examined, and a self-compensating method was presented. A relatively linear sensitivity of 500 V/(Nm) with little hysteresis was measured. In addition, the output response of the sensor was found to be nearly independent of the rotational frequency.

Bonding a thin ring of circumferentially polarized magnetostrictive material creates a near-perfect linear magnetic field with respect to input torsional stress (135). Garshelis and Conto (136) attached two magnetostrictive rings whose polarization directions are opposite to improve

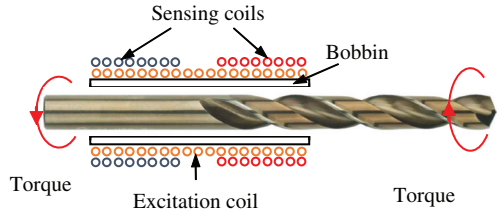

Figure 23. Noncontact measurement of torque on drill employing one excitation coil and two sensing coils one over the shank and one over the flutes (139).

sensitivity. Galfenol has higher magnetomechanical coupling than Ni or Ni alloys and thus greater potential torque sensing. Mahadevan (137) and Dapino hot formed a polycrystalline Galfenol sheet to a ring, where the magnetic domains initially have no preferred moment orientations. The ring-shaped Galfenol strip was bonded to a shaft using strain gauge adhesive. The varying permeability induced by torsional stress was measured by a fluxgate that consists of a driving coil and sensing coils. The maximum sensitivity achieved is ≈6.25 μV/με.

Sensor Shafts. These applications are examples of taking advantage of the magnetostrictive effects of the target material itself. In the first example, the in-process detection of the working torque on a drill bit is related to the drill permeability. An excitation coil surrounds part of the drill including the shank and the flutes, as shown in Figure 23 (138). Two sensing coils, one positioned over the flutes and one over the shank, are connected in series opposition allowing the measurement of the permeability. The permeability of the shank is less sensitive to changes in torque than the flutes, and the difference in the output voltages of the two coils changes in proportion to the applied torque. In the second example, a sensor shaft was made of Cr–Mo steel suitable for automobile transmission applications. Two grooved sections are surrounded by coils, which are configured in an AC bridge circuit. When torque is applied to the shaft, the Villari effect results in a change in impedance measured by the bridge. According to Shimada, this sensor design is robust with respect to temperature (139).

6.3. Motion Sensors

Bidirectional Magnetostrictive Transducers. The existence of the Villari effect makes it possible for a magnetostrictive transducer, such as those described in the sonar and motion/force device sections to have two modes of operation: transferring magnetic energy to mechanical energy (actuation) and transferring mechanical energy to magnetic energy (sensing). As with many other transducer technologies such as electromagnetic (moving coils) and piezoelectricity, magnetostrictive transduction is reciprocal and a transducer has the ability to both actuate and sense simultaneously. Applications such as the telephone and scanning sonar use this dual mode. For example, Terfenol-D sonar transducers can be used as either a transmitter or a receiver or both at the same time. Another potential use of dual-mode operation is in active

vibration and noise control. One transducer can be used to sense deleterious structural vibrations and provide the actuation force to suppress them. This approach to active control provides what is called colocated sensing and actuation, which aids in ensuring control system stability. Self-sensing control uses the sensed signal in a feedback loop to drive the transducer. Numerous papers have described systems based on this effect and shown its effectiveness (90,140,141).

Fenn and Gerver (142) have developed, tested, and modeled a velocity sensor based on a permanent magnet-biased Terfenol-D actuator. The output from the device was a voltage induced in a coil surrounding the monolithic Terfenol-D core, which was proportional to the time rate of change of the strain in the Terfenol-D core and ultimately the velocity of the connected target. Peak sensitivities of 183 Vs/m were seen when the coil was left open. In addition, the coil could be shunted to provide passive damping capability, and the voltage proportional to the target velocity could be monitored across the shunt resistor.

Noncontact Magnetostrictive Strain Sensors. Noncontact magnetostrictive strain sensors (NMASSs) use the magnetic field to couple the straining target to the sensing element. A noncontact system has several advantages (143). First, it is a noninvasive technique; that is, it does not require mechanical bonding to the target. This is a significant advantage for measuring strain of rotating targets. Second, the sensor can be moved to measure strain at different points easily and quickly, perhaps providing a three-dimensional strain-mapping capability. Finally, this sensor is rugged, with good sensitivity and overload capacity. Figure 22 shows the general configuration of the sensor (143) with the C-shaped ferromagnetic sensor core wound with an excitation and sensing coil. The flux path crosses the air gap to the target. Because of the magnetoelastic effect, strain in the target causes a change in the magnetic circuit permeability, which will be seen as a change in the sensed voltage. This sensor configuration has also been used to measure torque in shafts because the principal strains are 45° from the shaft axis.

The system discussed above utilizes the magnetoelastic coupling of the target itself to achieve noncontact strain measurement. For other nonmagnetic targets such as aluminum, a strain gauge made from strips of Metglass 2605SC has been developed by Wun-Fogle et al. (146). The permeability of the ribbons decreased in tension and increased in compression. The ribbons were prepared by annealing in a transverse 2.6 kOe magnetic field at 390 °C for 10 min and then rapidly cooled in a saturation magnetic field. To maintain their high sensitivity, the ribbons must be strongly bonded to the target in an initially stress-free condition. A highly viscous liquid bond was found to bond the ribbons to the target adequately, although it did result in a loss of DC response. For experimental verification, two ribbons were placed on the top and bottom of a beam and surrounded by two coils connected in opposition. The ribbons were excited by an external magnetic field of 1 kHz. The net voltage in the coil system was related to changes in permeability and, hence changes in strain of the ribbons. The strain measurement system resulted in a figure of merit, given by $F_\mu = (\partial\mu/\partial\epsilon)/\mu$, of 4×10^5, which compares favorably with conventional strain gauges. It was found that strains on the order of 10^{-9} could be measured at 0.05 Hz.

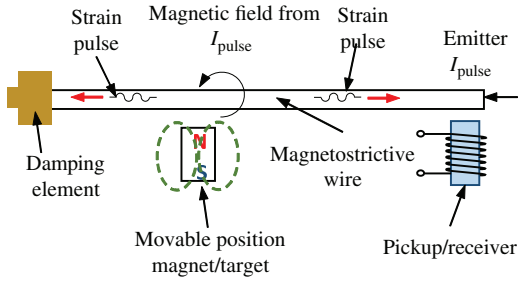

Figure 24. Magnetostrictive waveguide position sensor (130).

Magnetostrictive Position Sensors. Magnetostrictive waveguide position sensors detect the position of a permanent magnet connected to the target, which is free to move along the length of a magnetostrictive waveguide. An emitter is used to send a current pulse continuously through the waveguide, which produces a circumferential magnetic field. This combined with the longitudinal magnetic field produced by the permanent magnet results in a helical magnetic field.

The Wiedemann effect described earlier then results in a torsional strain pulse; the triggered torsional acoustic wave travels at the speed of sound in both direction away from the permanent magnet along the waveguide. One end of the waveguide is fitted with a receiver; at the other end, a damper attenuates the acoustic wave so that it will not reflect back corrupting the signal at the receiver and avoiding the development of standing waves. The receiver measures the time lapse between the current pulse and the acoustic wave, which is related to the distance between the receiver and the permanent magnetic/target. The acoustic wave can be measured by the change in permeability resulting from the strain pulse in the waveguide. In Figure 24, the receiver, or pick-up element, is shown as a magnetostrictive ribbon welded to the waveguide that converts the torsional pulse to a longitudinal elastic pulse. The permeability of the ribbon, which changes as a result of the elastic pulse, is monitored via Faraday's Law with a coil wrapped around the ribbon. A piezoelectric element can also be used as the receiver to measure the acoustic wave.

Several versions of this sensor are available commercially and discussed in the literature. Nyce (144) describes in detail the operation of MTS model LP. Current pulses with frequencies between 10 Hz and 10 kHz provide the excitation. The sensor performance is considered as a function of the magnetostrictive waveguide material (high magnetostriction, low attenuation, and temperature stability are desired) and geometry. Lucas Control System Products (the United Kingdom and the United States) has developed the MagneRule Plus, a compact position sensor for measurements up to 120 in. (305 cm) with high linearity and repeatability. In addition, it can measure fluid levels by connecting the permanent magnet to a float, which is

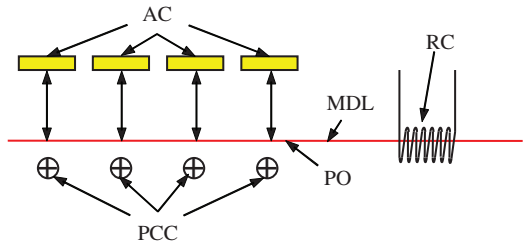

Figure 25. Magnetostrictive delay line with active core connected to target, pulsed current conductor, receiving coil, and point of origin (PO) for acoustic stress (108).

then placed in the fluid to be monitored. Finally, Equipel (France) manufactures and sells Captosonic position sensors capable of measuring distances up to 50 m with ±1 mm accuracy (145).

Magnetostrictive waveguide sensors measure position at the millimeter scale over a range of meters. On the other hand, magnetostrictive delay lines (MDLs), as shown in Figure 25, are able to detect position change at the micrometer scale within a narrow range. An acoustic pulse is propagated through the magnetostrictive delay line and detected by a receiving unit. A current pulse through a conductor (PCC) orthogonal to the magnetostrictive delay line (MDL) generates a pulsed magnetic field in the MDL, which generates an elastic wave (see Figure 25). An active core of soft magnetic material, placed near the PCC, is connected to the target and is free to move relative to the MDL. The magnetic pulse and hence elastic wave generated in the MDL is sensitive to the magnetic coupling between the active core and MDL. As the target and active core move away from the MDL, the magnetic coupling between the PCC and MDL increases, so the magnetic pulse and elastic wave in the MDL increases in strength. The output to the sensor is the pulse generated in the receiving unit coil (RC) as described by Faraday's law. The output voltage induced in the RC is sensitive to the gap distance between the MDL and active core; for MDL–active core, displacement is less than 2 mm. Most importantly, the output is fairly linear and anhysteretic with respect to the MDL—active core displacement. Sensitivities of 10 μV/μm have been reported using 24 μm thick Metglas 2605SC amorphous ribbon as the MDL (108). Permanent magnets were also used to maximize the generation of the acoustic pulse and the measured voltage in the RC. Multiple active core–PCC elements can be used with one MDL to form an integrated array. This novel aspect of the sensor system and several active core-–PCC–MDL configurations are discussed by Hristoforou and Reilly (147). Applications for this sensor include tactile arrays, digitizers, and structural deformations.

Angular Speed Sensor and Gyro Sensor. A miniature gyro sensor is essential for handheld cameras, navigation systems, and cellphones to detect rotational motion and track device orientation. Yoo et al. (148) developed a microgyro sensor based on a Galfenol tuning fork resonator, as shown in Figure 26. Similar to the Galfenol unimorph actuator discussed in Section 5.4.3, the left prong (driving prong) bends in the $x - z$ plane when a driving voltage V_D energizes the left coil. Due to the sympathetic resonance, the right prong (sensing prong) also fluctuates in the $x - z$ plane at the same frequency, as shown in Figure 27a. When a rotation around the z-axis starts, the Coriolis force, which is proportional to the rotation speed, induces out-of-plane bending (bending in the $y - z$ plane). This out-of-plane bending creates longitudinal stress variation, causes flux density variation in the Galfenol stripe on the sensing prong, and thus creates a voltage signal V_s due to Faraday's law. Marschner et al. (149) later added permanent magnets on the tip of each prong to improve the device's sensitivity.

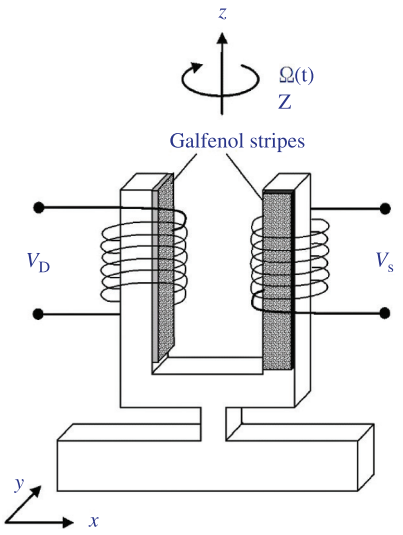

Figure 26. Configuration of Galfenol gyroscopic sensor (148).

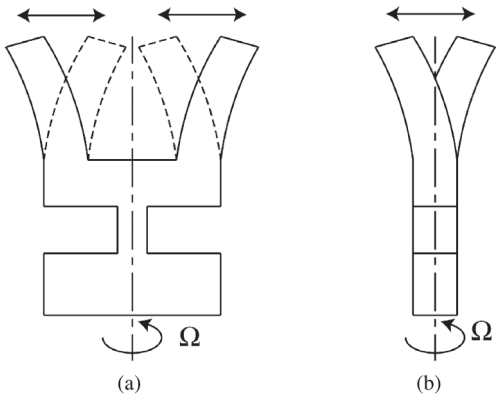

Figure 27. (a) Driving mode. (b) Sensing mode (148).

6.4. Force Sensors

Magnetostrictive Delay Lines. The magnetostrictive delay line displacement sensor configuration has been modified to produce a force distribution sensor (150,151). A force applied directly to the MDL will distort the acoustic signal by the emitter as described previously. The change in the acoustic wave measured by a receiver coil is related to the force applied to the delay line. An experimental device tested by Hristoforou and Reilly (150) used a Metglas 2605SC FeSiBC amorphous ribbon as the delay line

embedded in a fiberglass channel. The channel bends under an applied force, stressing the MDL. In addition, the channel ensures that the PCC oriented perpendicular to the MDL ribbon on the bottom of the channel does not move relative to the MDL. For a given current, the voltage detected by the receiver coil caused by a force F is proportional to the e^{-cF}, with calibration constant c. Integrated arrays for measuring force can be constructed with multiple MDL (each with a receiver) and PCC oriented perpendicularly. The values of multiple forces on the two-dimensional array can be backed out from the voltages measured by the receivers.

Magnetostrictive Force Sensor. The magnetic permeability of magnetostrictive materials is sensitive to stress in the material (152,153). This concept has been applied to force sensors. Kleinke and Uras describe a force sensor that employs the change in electrical impedance of a coil that is flux linked to a magnetic circuit to measure the stress or force acting on a magnetostrictive component in the magnetic circuit (154). It is similar in construction to the noncontact magnetostrictive strain sensor discussed earlier. However, rather than having a C shape, two magnetostrictive cores are held in place by rigid end pieces (see Figure 28). A coil surrounds each core, one of which is used for excitation and the other for sensing. A constant amplitude AC is impressed in the excitation coil generating an oscillating magnetic field. This results in a voltage in the detection coil with a magnitude proportional to the time rate of change of flux linking the detection coil. An applied force on the sensor will cause a strain change in the magnetostrictive cores resulting in a change in the core magnetization. In this mode, where the magnetomotive force is kept constant, a change in the output voltage from the detection coil is linearly related to the change in force. In a constant flux operation mode, the excitation current is allowed to vary in order to maintain a constant detection coil output voltage. In this case the change in excitation current is related to the change in force. The configuration shown in Figure 28 was improved by Uras (155) such that only a single coil was needed to excite the magnetostrictive material and to detect the permeability change. Baudendistel and Turner (156) later embedded the excitation and sensing coils (only one turn for each) in a magnetostrictive ring and created a self-inductance force sensor with reduced measurement noise. Compared with conventional force transducers such as those that employ strain gauges, this magnetostrictive force sensor is simpler, more rugged, relatively inexpensive, and employs simpler electronics. The configuration of magnetostrictive force sensors varies depending on particular application requirements. For example, Baudendistel and Turner (156) embedded copper wires in a magnetostrictive ring and created a self-inductance force sensor to reduce noise.

The magnetostrictive force sensors discussed above require bulky excitation and detection coils. Day et al. (116) recently proposed a more compact configuration, which is shown in Figure 29. A long and thin Galfenol strip mimicking mammalian whiskers or vibrissae is constructed as a cantilever. A permanent magnet attached to the fixture side provides bias magnetic field through the Galfenol

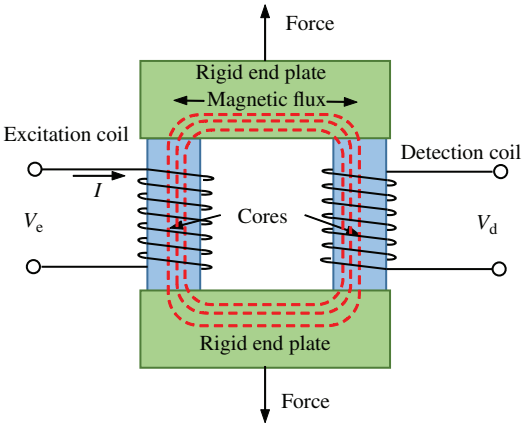

Figure 28. Magnetostrictive sensor for measuring force, composed of two ferromagnetic cores, one with an excitation coil and the other with a sensing coil, between two rigid end plates (115).

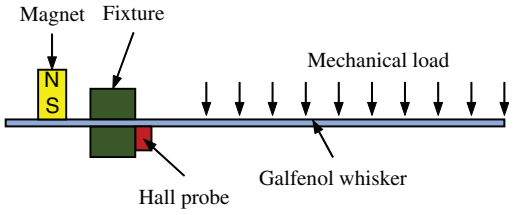

Figure 29. Configuration of Galfenol whisker sensors measuring the flow rate (116).

strip. The mechanical load, for example, the force induced by flowing water, induces stress variation in the Galfenol whisker, varies the permeability of Galfenol, and, therefore, changes the magnetic field around the hall chip. The flow rate, which is related to the mechanical load, can thus be measured from the varying hall chip output. Compared with Galfenol, aluminum and iron alloys, or Alfenol, is much cheaper and more flexible while exhibiting moderate magnetostriction (about 176 microstrain) (117). Similar whisker-type force sensors based on Alfenol have been validated in experiments (118).

Amorphous Ribbon Sensors. A tensile force sensor based on the strong Villari effect of amorphous ribbons, such as Ni-, Fe-, and Co-based alloys, has been described by Seekircher and Hoffmann (157). A transmitting coil excites the ribbon, while a pair of detection coils measure the maximum induction, which is dependent on the stress as shown in Figure 30. Loads below 4 N were measured with Co alloy ribbon, 25 μm thick by 3 mm wide with negligible hysteresis. The high Young's modulus of the ribbons results in low-displacement sensors, which can be load-bearing elements. In some cases, temperature compensation is required.

Numerous torque sensor designs, patents, and literature are also available. Highly sensitive shock–stress sensors employing iron-rich amorphous ribbons are described in detail by Mohri and Takeuchi (159). A combined torque–force sensor has also been developed (160). The change in permeability (or magnetic flux) in a magnetic circuit

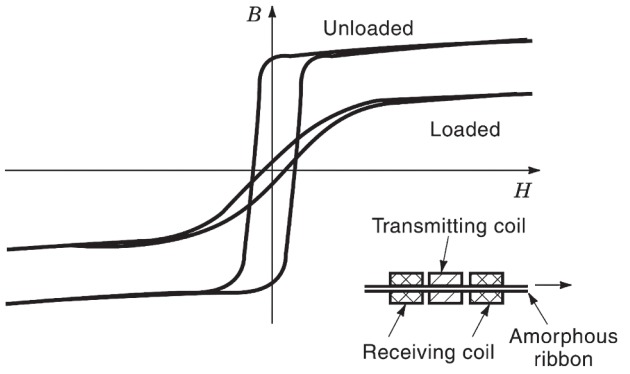

Figure 30. Amorphous ribbon force sensor with one excitation coil and two receiving coils so that changes in permeability caused by a force are detected (158).

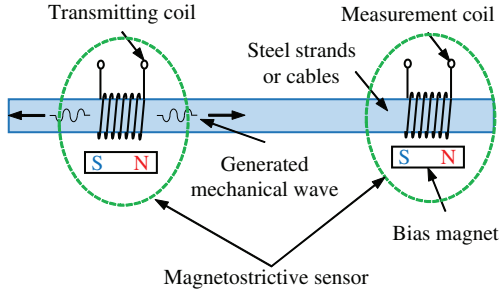

Figure 31. Magnetostrictive sensor for characterizing corrosion and monitoring ferromagnetic materials such as pipes and strands (164).

resulting from strain in an element of the circuit can be used to measure both torque as described previously and force.

6.5. Nondestructive Examination (NDE)

Figure 31 shows a noncontact sensor that uses the magnetostrictive properties of the target material to excite elastic waves that can be measured and monitored for use in characterizing the target material properties (161–163). The system can be used only with ferromagnetic material that has a magnetoelastic response. The sensor consists of a transmitting coil (pulse generator, power amplifier, and bias magnet) surrounding the object, which generates the mechanical wave via magnetostrictive excitation. A receiving coil (signal preamplifier, data acquisition hardware, and permanent magnet) located at a distance from the excitation coil measures the signal produced by the waves. These signals can be used to characterize the material for corrosion, measure stress in strands, and so on. Signals are generated by changes in the material geometry. Experimentation has shown that the wave attenuation increases with the degree of corrosion. This method has been used successfully to identify corrosion in strands, reinforced bars (including those embedded in cement), water pipes, and other systems where noninvasive monitoring techniques are preferred.

Similar concepts have been successfully applied to nondestructive examination (NDE). Kim and Kim (165) invented a Terfenol-D-based crack detector mounted on the

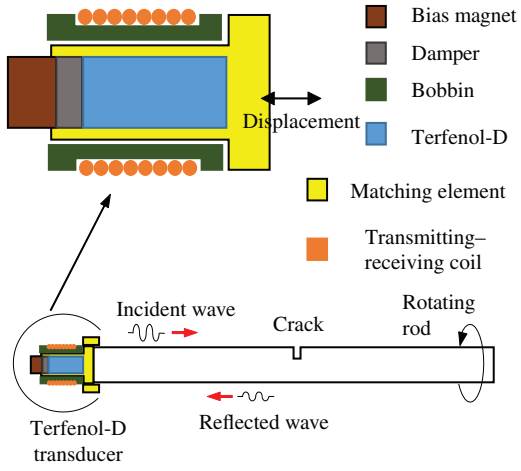

Figure 32. Schematic diagram of the Terfenol-D transducer for shaft damage detection (164).

tip of a rotating shaft, as shown in Figure 32. A current pulse through the coil energizes the Terfenol-D stack and generates a longitudinal wave (the incident wave) propagating along the shaft axis. The incident wave is reflected by any cracks inside the shaft. The reflected wave returns to the Terfenol-D stack and induces mechanical deformation, which can be converted to electrical voltage on the coil. The time difference between the current pulse and the electrical voltage induced by the reflected wave determines the location of cracks. Wang et al. (166) replaced the Terfenol-D stack in Figure 32 with Galfenol and excited ultrasonic waves instead of impulsive waves inside the shaft to improve detection accuracy. Since the Terfenol-D or Galfenol component rotates together with the shaft and couples wirelessly with the transmitting–receiving coil, the crack detection procedure is contactless and essentially takes place in real time.

6.6. Magnetometer

There are numerous designs for magnetic field sensors, including many that rely on magnetostrictive properties of component materials. These sensors vary considerably, in part because they are designed to detect magnetic fields of different strengths and frequencies (167).

The first magnetometer design, developed by Chung et al. (168–170), employs a Terfenol-D sample to convert a magnetic field into a measurable quantity. A Terfenol-D rod strains in the presence of an AC magnetic field. This displacement can be measured accurately with a laser interferometer calibrated to output a signal related to the magnetic field. A DC magnetic bias is used to optimize the sensitivity of the Terfenol-D strain with magnetic field, resulting in values of up to 10^{-6} /G. In addition, the sensitivity was found to be a function of the mechanical prestress.

Magnetoelectric composites consisting of laminated magnetostrictive materials bonded to piezoelectric layers have been implemented in magnetic field sensing. Dong et al. (129) presented a ring-shaped magnetoelectric magnetic field sensor, illustrated in Figure 33. The magnetic

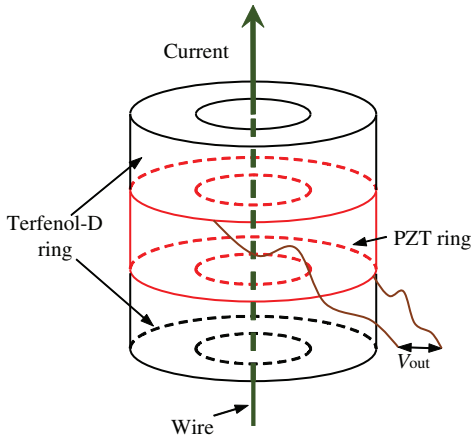

Figure 33. Vortex magnetic field sensor (129).

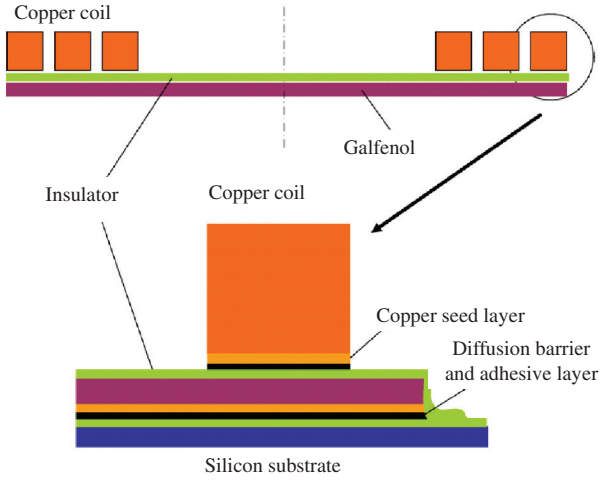

Figure 34. Galfenol thin-film sensors. (Reprinted with permission from Reference 177. Copyright 2009, Elsevier.)

domains in the Terfenol-D rings are oriented circumferentially; the PZT ring is polarized circumferentially. The Terfenol-D layer strains in the presence of a vortex magnetic field. The mechanical deformation is then transferred to the PZT ring and converted to a voltage signal. Zhai et al. (171) bonded flexible Metglas with piezoelectric fiber and developed a geomagnetic sensor achieving a resolution of 8×10^{-6} Oe over ±1.5 Oe range.

Other magnetic field sensors combing magnetostrictive materials and optic fibers are also available. In 1979, Yariv and Winsor proposed a now common configuration that uses a magnetostrictive film coating applied to an optic fiber (172). The magnetic field causes the magnetostrictive film to deform, straining the optic fiber. This causes changes in the optical path length and the phase of the laser light passing through the optic fiber, which can be detected by an interferometer. Mermelstein shows that the resolution limit at DC to low frequency (less than 1 Hz) of such a sensor is approximately 3×10^{-11} Oe (173). Magnetostrictive amorphous metals, often in the form of ribbons, are extremely sensitive to external magnetic fields and have been used as the active element of a magnetometer (133). Also, a magnetic field sensor has been developed based on magnetostrictive delay line technology (174). Bragg grating fibers (FBGs) have been embedded in a magnetostrictive composite (Terfenol-D particles dispersed in a plastic matrix), thus creating a small size magnetic field sensor for severe corrosive environments. The magnetic composites expand in the magnetic field, strain the FBGs, and thus change the wavelength of the light reflected by the gratings. By measuring the spectral response of transmitted light, this magnetic field sensor was shown to achieve a high sensitivity of 3 Oe in static and dynamic conditions (175).

6.7. Microscale and Nanoscale Sensors

Manufacturing efforts have led to a reduction in the size and cost of magnetostrictive sensors, enabling small- scale sensors in the form of films or fibers (176). Galfenol is particularly well suited for deposition at small scales. Wenzel et al. (177) developed a microscale force sensor by bonding a thin Galfenol layer (1–2 mm thick) to a silicon substrate, as shown in Figure 34. The copper coil and the magnetically conductive Galfenol layer form a variable inductor. The bending of a Galfenol–silicon composite beam induces tensile stress in the Galfenol layer, changes the Galfenol layer's permeability, and varies the inductance of the variable inductor. The sensor's electrical resonance, which depends on the coil inductance, can be measured by an electrical network analyzer. Wenzel et al. (177) glued the sensor with a 23-turn coil (2 mm × 10 mm) on a titanium cantilever to measure the tip force. A linear sensitivity of 1 kHz/N was achieved over a force range of 8 N.

The same principle was implemented in medical applications. Sauer et al. (178) presented a microscale Galfenol–silicon film coupled with a copper coil to track the bone fracture healing process, as shown in Figure 35. As the bone fracture heals, the physical load gradually transfers from the osteosynthesis plate to the bone tissue, thus creating stress in the thin Galfenol film. The inductance of the copper coil, which depends on the stress state of the Galfenol element, is then measured by an electrical network analyzer. This thin Galfenol–silicon film sensor provides a convenient, cheap, wireless, and accurate method to measure strain and stress variation.

Another type of magnetostrictive sensor mimics the inner ear's cilia and cochlea. McGary et al. (10) fabricated high-aspect-ratio Galfenol nanowires with diameters varying from 100 to 200 nm and lengths up to 60 mm on different substrates using electrochemical deposition technology. The force or acoustic inputs create flux density variation in Galfenol, which can be measured by magnetoresistive sensors. The magnetostrictive nanowire concept is applicable to underwater sonar and medical scanning.

6.8. Magnetostrictive Dampers and Energy Havesters

Magnetostrictive materials are able to dissipate mechanical energy input through intrinsic hysteresis, stress-induced eddy current, and mechanical–magnetic energy coupling, and thus can be implemented as mechanical dampers. Since Terfenol-D is prone to failure in

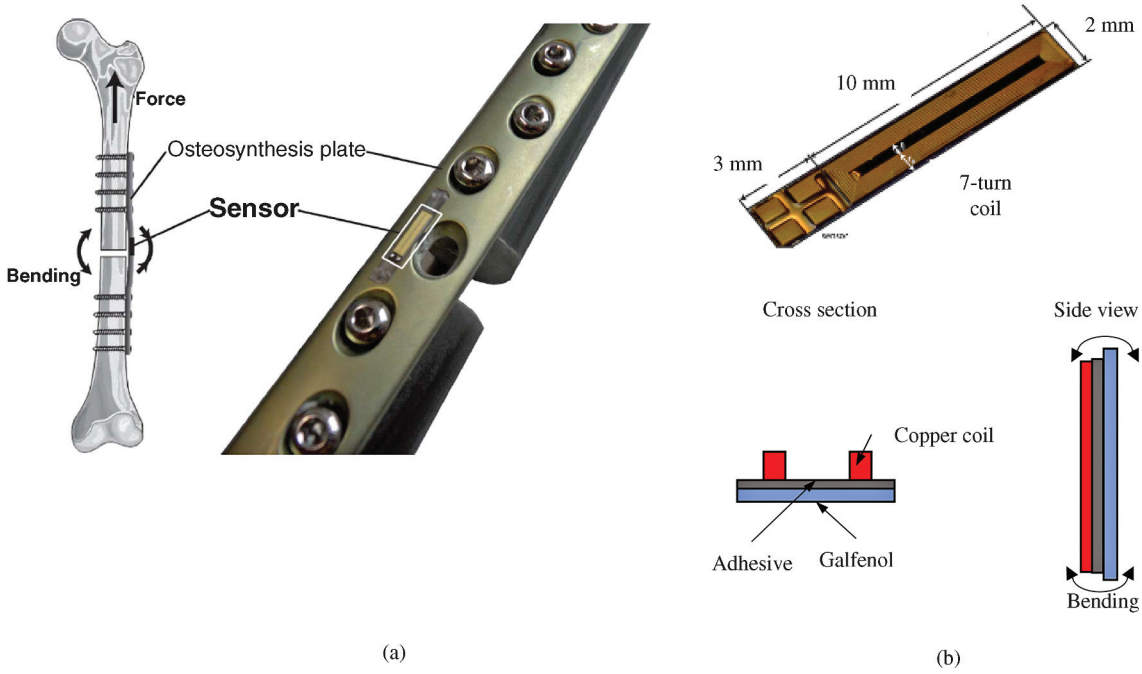

Figure 35. (a) Osteosynthesis plate with Galfenol-based strain sensor. (b) Geometry of Galfenol strain sensor. (Reprinted with permission from Reference 178. Copyright 2012, IEEE.)

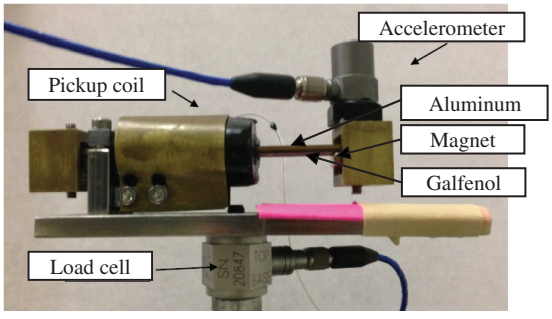

Figure 36. Galfenol unimorph shunted damper (181).

tension or in torsion, early Terfenol-D-based dampers either required complicated protection mechanisms (179) or consisted of Terfenol-D particles embedded in polymer matrices (180). Hence, the performance and applications of Terfenol-D dampers are limited. Galfenol dampers, on the other hand, exhibit mechanical robustness and thus can be placed directly in mechanical load paths. Murray and Yoo (181) developed a Galfenol-shunted damper in bending mode (Figure 36) and achieved over 900% damping increment at resonance by tuning the electrical impedance attached to the coil.

Shunted magnetostrictive dampers convert mechanical energy to electrical energy, which is dissipated in resistive loads as heat. Through replacing the resistive load with supercapacitors or batteries, electrical energy can be stored; the shunted dampers are transformed to energy harvesters. Energy harvesters have gained interest due to the reduction in size and power consumption of embedded and wireless sensors. Berbyuk (182) designed a Galfenol-based energy harvester, which requires large axial force, as shown in Figure 37. Magnetostrictive harvesters are often configured as cantilever beams that are able to scavenge energy from structural vibrations. Deng and Dapino (183) presented a Galfenol-based unimorph energy harvester, as shown in Figure 38a. Sinusoidal base vibrations excite significant tip deflection around the beam's resonance. The passive stainless steel substrate pushes the Galfenol layer away from the unimorph's midplane, such that the Galfenol bears purely tensile or compressive stress during bending. The flux density variation induced by the stress variation is then converted to electrical energy on the pickup coil. Deng and Dapino (183) achieved an average output power density of 63.6 mW/cm^3 for a 200 Hz, 9.8 m/s^2 sinusoidal base excitation. Ueno and Yamada (185) constructed a bimorph harvester by replacing the passive stainless steel layer with another Galfenol beam, as shown in Figure 38b. Wang and Yuan (184) replaced the Galfenol layer with Metglas in the unimorph configuration and obtained an output power density of 0.9 mW/cm^3 for a 58 Hz, 8.06 m/s^2 sinusoidal base excitation. The literature therefore suggests that energy harvesters based on magnetostrictive materials achieve power densities similar to piezoelectric harvesters. However, harvesters based on magnetostrictive materials suffer no depolarization issues and have a favorably low output impedance.

6.9. Miscellaneous

Magnetostrictive sensors have been used to measure or monitor a number of other properties and characteristics. Some examples found in the literature include hearing aids (121), magnetoelastic delay line digitizers (186), magnetoacoustic keyboards (187), thermometers (188), biomedical monitors for lung ventilation (189), liquid viscosity

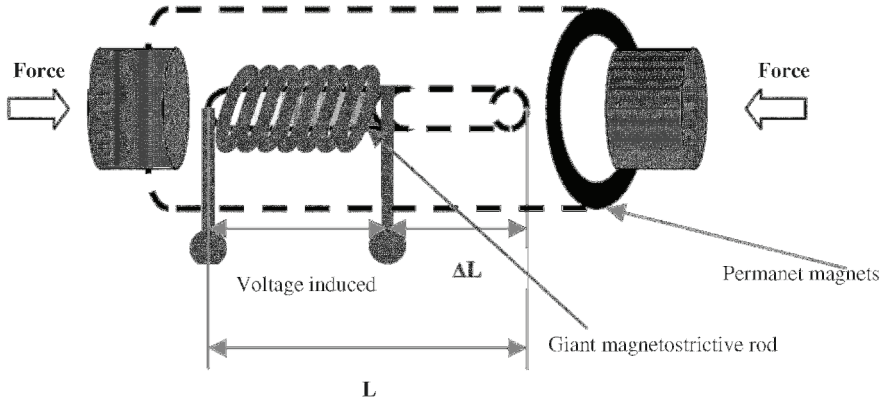

Figure 37. Schematic of the Galfenol energy harvester in axial mode. (Reprinted with permission from Reference 182, Copyright 2013, SPIE.)

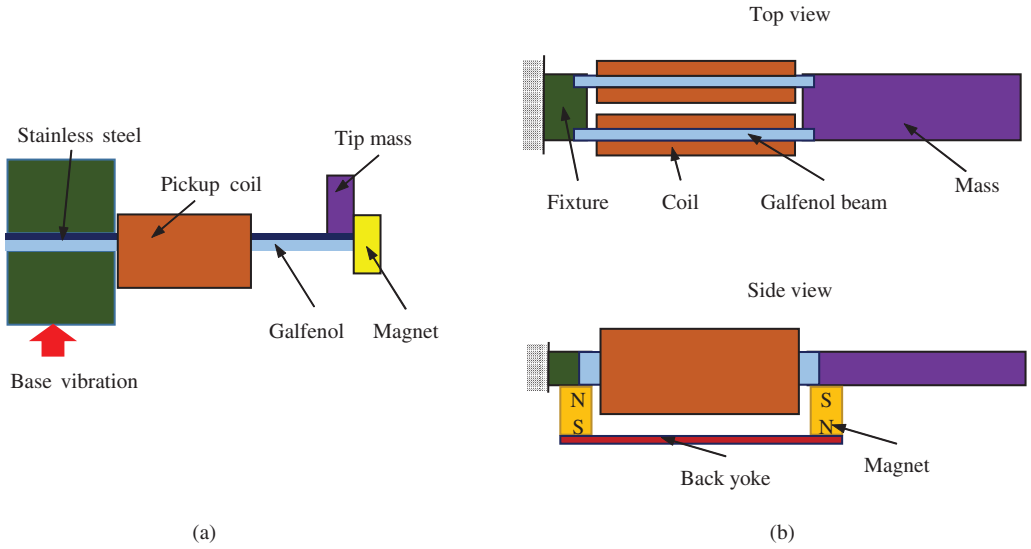

Figure 38. (a) Galfenol unimorph energy harvester (183). (b) Galfenol bimorph energy harvester (185).

and density sensors (190), ethanol concentration measurement (191) and spine movement (192), bimorphs for two-dimensional scanning elements (158), and composite cure monitors. An interesting review of additional sensors is given by Restorff (124).

7. MAGNETOSTRICTIVE DEVICE MODELING

The increased use of magnetostrictive materials has not been accompanied by the availability of complete and accurate transducer models. Complete models must incorporate the different operating regimes present in magnetostrictive transducers in a manner compatible with the requirements of specific applications. The regimes present in magnetostrictive transducers are electric (which involves routing of magnetic field through magnetic circuit for magnetization of the magnetostrictive core), mechanical (elastic state of the materials present in the transducer), and thermal (the temperature distribution in the transducer materials). Extensive experimental evidence (41,50,53) demonstrates that it is crucial to consider the interaction between these regimes; therefore, models for the various regimes need to be coupled to provide a complete description of a transducer system.

Most of the currently available models of magnetostrictive transducers fail to incorporate all regimes simultaneously. This is in part because transducer models are still predominantly based on the linear constitutive piezomagnetic equations (Eq. 1) (23). These equations neglect the effects of coupling between stress, magnetization, and temperature in the material, which have a bearing on the mechanical performance, as indicated in Reference 57, among others.

Carman and Mitrovic (164) and Kannan and Dasgupta (193) extended the scope of the linear constitutive equations by including specific nonlinear effects. The nonlinear dynamics of magnetostrictive transducers has also been modeled following a phenomenological approach. One such approach is obtained through the use of

generalized Preisach operators. Preisach models that specifically target giant magnetostrictive materials are discussed by Restorff et al. (194), Adly and Mayergoyz (195), and Smith (196). These models characterize different operating regimes but are cumbersome to implement in magnetostrictive transducers where performance changes significantly during operation.

Other modeling efforts have combined physical laws with phenomenological observation. Engdahl and Berqvist (197) present a model capable of dealing with nonlinearities and various losses, such as magnetomechanical hysteresis, eddy currents, ohmic heating, and mechanical losses. Physically based Preisach models combined the empirical robustness of nonphysical laws with some understanding of the physical processes that govern magnetic and magnetostrictive hysteresis. Basso and Bertotti (198), for instance, developed a Preisach-based hysteresis model for materials where the magnetization is dominated by domain wall motion.

Nevertheless, there does not exist a fundamental model applicable to the complete performance space of magnetostrictive transducers. The development of physically-based models that incorporate the different operating regimes and the issues inherent to them will certainly extend the utility of these transducers. In this section, some of the fundamental issues in magnetostrictive transducer modeling are identified, and some of the current state-of-the-art modeling techniques that handle these different issues are reviewed.

7.1. Linear Transduction

The linear transduction equations provide a "black box" model of the relationship between electrical and mechanical sides of the transducer through the transducer's total electrical impedance. These equations can be written as

$$V = Z_e I + T_{em} v \tag{16a}$$

$$F = T_{me} I + z_m v \tag{16b}$$

where V and I are voltage and current across transducer leads, respectively Z_e is the blocked electrical impedance, v is the velocity, T_{em} and T_{me} are electrical due to mechanical and the mechanical due to electrical transduction coefficients, and z_m is mechanical impedance. Hunt, Rossi, and many others have authored authoritative texts on the subject of transduction covering the use of equivalent circuit models such as that presented in Figure 8b and the transduction equations as applied to modeling of magnetostrictive devices.

7.2. Magnetization

Magnetization and the magnetoelastic interactions taking place inside the magnetostrictive core and other transducer components have been modeled in different manners. Transducer magnetic models can be formulated using standard techniques (see *magnetic circuits*) (i.e., using equivalent circuit representations and/or finite-element modeling approaches). The least well-defined component of such models is inevitably the magnetic state of the magnetostrictive core, which, referring back to Figure 3, changes significantly with operating conditions.

One approach for modeling a magnetostrictive material is to consider the material at its micromagnetics level. Classical micromagnetics work by Brown (199) assumes that the material is simultaneously magnetizable and deformable with its energy state defined by elasticity, thermodynamics, and electromagnetic principles. Recent work in this field deals specifically with Terfenol-D (200). Although the modeling results are useful at the domain level, the extension of micromagnetic models to describe the performance of transducers is a major undertaking.

The Preisach model has been used extensively for characterization of ferromagnetic materials, and more recently for characterization of magnetostrictives as well. Much research effort has been devoted to accommodate physical aspects into the Preisach approach, which in its original form cannot be traced back to fundamental principles. Reimers and Della Torre implement in Reference 201 a fast inverse hysteresis model amenable to control applications and with applicability to magnetostrictive materials.

Following the classical anisotropy domain rotation model by Stoner and Wohlfarth (202), Lee and Bishop (203) extended their idea to a random assembly of domain particles having cubic anisotropy. Clark et al. (204) included compressive loading along the [1 1 1] easy axis direction in a two-dimensional scheme. Jiles and Thoelke (205) generalized this model to three dimensions, by considering the anisotropy, magnetoelastic, and field energies along all three directions. Although model results are in good agreement with measured data, the identification of the fractional occupancies, which define the participation of different easy axes in the total magnetization, is by no means trivial.

Another modeling approach that yields significant results is the ferromagnetic hysteresis model. Theory by Jiles and Atherton (206) predicts quasi-static magnetization-applied field (M-H) loops in ferromagnetic materials by considering the energy of domain walls as they bow and translate during magnetization. Later extensions include models of magnetostriction, eddy current losses, minor loops, and mechanical prestress (see Reference 62). The appeal of the Jiles–Atherton model stems from the physical basis of the model parameters and the fact that only five parameters are needed for complete description of the magnetic state of the material. However, this model is purely magnetic in nature, which highlights the need for accurate and general magnetomechanical characterization laws to describe the transduction process in the transducer completely.

7.3. Stress

It is common practice to place giant magnetostrictive samples under a mechanical compressive prestress for operation. The ability of the material to survive high accelerations and shock conditions improves under compressive stress because, for example, Terfenol-D is much more brittle in tension (tensile strength ≈28 MPa) than in compression (compressive strength ≈700 MPa) (54). Under dynamic operating conditions in systems using the more

brittle magnetostrictives such as monolithic Terfenol-D, the rated system output force is usually limited by the magnitude of the device prestress according to Newton's Second Law, where $F = ma = \sigma_0 A$. Above the prestress, the output dynamic load will accelerate away from the magnetostrictive driver, only to return with potentially damaging results. In addition, adequate preloading is capable of improving the magnetic state in the material as a consequence of the coupling between the magnetic and mechanical states. Figure 9c shows transducer electrical impedance function sensitivity to changes in prestress.

Considering an energy balance in the material, the mechanical prestress is an additional source of anisotropy energy that competes against the magnetocrystalline anisotropy, strain, and applied field energies. The application of the compressive preload forces a larger population of magnetization vectors to align perpendicular to the direction of application of the preload, where a state of local minimum energy is reached. This translates into both a smaller demagnetized length and increased saturation magnetostriction. However, for compressive preloads larger than a certain value, the prestress energy overpowers the elastic energy produced by the material and the magnetostriction decreases.

The relationship $\epsilon - M$ in Terfenol-D has been reported to be nearly independent of prestress except for very low prestresses and high magnetizations. Clark et al. (207) report a range of about 15–55 MPa for the $\epsilon - M$ stress independence in Bridgman-grown samples. In addition, work by Kvarnsjö (97) indicates that at high prestresses, the primary magnetization mechanism is domain magnetization rotation; as a consequence, the quadratic law for magnetostriction discussed earlier is appropriate. Clark et al. (207) found that the quadratic law is incorrect in the low-prestress regime (below 30 MPa for statically loaded, single-crystal material) where it was found that strain depends directly on stress and that the magnetostriction cannot be accounted for by a single-valued magnetization law (i.e., hysteresis is observed).

7.4. Thermal Effects

Temperature effects can be incorporated in the linear piezomagnetic model given in equation 1. Furthermore, by considering higher order interactions between magnetization, stress, and temperature, Carman and Mitovic (164) developed a model capable of producing results in good agreement with experimental data at high preloads. However, the model is not capable of predicting saturation effects. Following the lead of Hom and Shankar, (208) Duenas et al. (23) developed an analogous set of constitutive equations for magnetostriction. These equations are given by

$$\epsilon_{ij} = s^{M,T}_{ijkl}\sigma_{kl} + Q^{T}_{ijkl}M_k M_l + \alpha^{M}_{ij}\Delta T \tag{17a}$$

$$H_k = -2Q^{T}_{ijkl}M_l\sigma_{ij} + \frac{M_k}{k|M|}\operatorname{arcranh}\left(\frac{|M|}{M_s}\right) + P^{\sigma}_{k}\Delta T \tag{17b}$$

where ϵ is the strain, s is the compliance, Q is the magnetostrictive parameter, M and M_s are magnetization and saturation magnetization, α is the coefficient of thermal expansion, T is the temperature, H is the magnetic field, P is the pyromagnetic coefficient, and k is the constant. Superscripts indicate the constant physical condition under which the parameter is measured, and subscripts indicate tensor order following conventional notation. This model successfully captures the quadratic nature of magnetostriction for low to medium field levels, but it does not completely describe the saturation characteristics. The model allows the incorporation of magnetostrictive hysteresis via complex model parameters.

Heat not only affects the magnetization processes in the magnetostrictive core but also has bearing on the overall transducer design. Together with magnetomechanical hysteresis and eddy current losses, ohmic heating in the excitation coil is perhaps one of the most significant sources of losses. Other thermal effects to consider in transducer design are thermal expansion of the magnetostrictive driver itself [for Terfenol-D, $\alpha \approx 12 \times 10^{-6}/^{\circ}\mathrm{C}$ (54)], dependence of material properties and performance of Terfenol-D on temperature, thermal expansion of the coil (coils used in prototype transducers showed expansion above 1.5% when heated from room temperature to temperatures of around 100 °C), thermal expansion of other transducer components, and the thermal range of the coil insulation. Maintaining controlled temperatures during operation is critical for certain transducer applications. One clear example of this is precision machining. Transducers for this type of application need to use efficient thermal sinks, either active (cooling fluids) or passive (thermally conducting materials, superconducting solenoids), or a combination of the two.

7.5. Thermodynamic Constitutive Models for Magnetostrictive Materials

Constitutive models for magnetostrictive materials must describe material nonlinearities (hysteresis, saturation, and anisotropy) and the coupling of mechanical and magnetic energies. Mathematical models such as the Preisach model (209) and the Prandtl–Ishlinskii model (210) are built on phenomenological operators, thus requiring large amounts of parameters to be measured. Magnetostrictive material models based on thermodynamic energy principles, which are computationally efficient, have been developed. Armstrong (211) first assumed the bulk magnetization M and magnetostriction S_m are weighted sums of local responses:

$$M = M_s \sum_{k=1}^{r} \xi^k m^k, \quad S_m = \sum_{k=1}^{r} \xi^k S^k_m \tag{18}$$

where ξ^k is the weight or volume fraction of the kth easy direction, r is the total number of possible magnetic moment orientations, and m^k and S^k are the magnetic moment orientation and local magnetostriction of the kth easy direction, respectively.

A magnetic moment tends to be oriented along the direction m^k where the Gibbs energy or magnetic free energy is a minimum. The Gibbs energy consists of three terms: anisotropy energy, magnetic energy, and magnetomechanical energy. For cubic symmetric Galfenol, the surface plot

of Gibbs energy for a single magnetic domain was presented by Evans and Dapino (212). As shown in Figure 39a, magnetic moments are initially oriented along the *x*-*y*-, and *z*-axes. The applied magnetic field creates a local minimum in the field's direction, thus magnetic moments tend to be aligned along the magnetic field; the applied stress create four local minima that are perpendicular to the stress direction, so the magnetic moments tend to rotate away from the stress direction.

To smooth the magnetization calculations, an energy-based Boltzmann distribution was implemented to calculate the volume fraction as

$$\xi^k = \frac{e^{-G^k/\Omega}}{\sum_{k=1}^{r} e^{-G^k/\Omega}} \tag{19}$$

where Ω is the Armstrong smoothing factor and G^k is the Gibbs energy of kth easy direction (214).

7.6. AC or Eddy Current Losses

Dynamic operation leads to additional complications in the performance of magnetostrictive transducers. One important loss factor to consider is the eddy (or Foucault) currents. As modeled by the Faraday–Lenz law, eddy currents are set up in the transducer's conducting materials to resist magnetic flux changes. These currents produce a magnetic flux that resists the externally applied magnetic field and simultaneously cause a nonuniform distribution of current density often known as skin effect. Classical eddy current power loss formulations assume complete magnetic flux penetration and homogeneous permeability throughout the material. This assumption is valid only for thin laminates; hence, it is invalid for thick solid cylindrical transducer cores. The characteristic frequency above which the homogeneity of penetration of the magnetic flux is compromised, for cylindrical samples, is given by

$$f_c = \frac{2\rho}{\pi D^2 \mu^\epsilon} \tag{20}$$

where ρ is the resistivity of the material ($\rho \approx 0.6 \times 10^{-6}\ \Omega\cdot$ m for Terfenol-D (170)), D is the rod diameter, and μ^ϵ is the clamped permeability. For a 6.35 mm (0.25 in.) diameter rod, the characteristic frequency is about 5 kHz. Laminations in the magnetostrictive core, low operating frequencies, silicon steel end caps, and slit permanent magnets help to mitigate the effects of eddy currents.

A modeling approach based on energy considerations is shown by Jiles (215). This approach considers eddy currents as a perturbation to the quasi-static hysteresis. The simplicity of this model is, however, offset by the limitations imposed by its assumptions. Because uniform flux penetration is assumed, its applicability is limited to thinly laminated material or low operating frequencies.

Another classical approach to the eddy currents issue is the one presented by Bozorth (14) among others. In this model, a so-called eddy current factor X is used to account for the reduced inductance caused by the oppositely induced magnetic field. The complex quantity $X = X_r + jX_i$ can be written for cylindrical current-carrying conductors in terms of Kelvin ber and bei functions and is dependent upon frequency of operation f and the characteristic frequency f_c as follows:

$$X_r = \frac{2}{\sqrt{p}}\left(\frac{\mathrm{ber}\sqrt{p}\,\mathrm{bei}'\sqrt{p} - \mathrm{bei}\sqrt{p}\,\mathrm{ber}'\sqrt{p}}{\mathrm{ber}^2\sqrt{p} + \mathrm{bei}^2\sqrt{p}}\right) \tag{21a}$$

$$X_i = \frac{2}{\sqrt{p}}\left(\frac{\mathrm{ber}\sqrt{p}\,\mathrm{ber}'\sqrt{p} - \mathrm{bei}\sqrt{p}\,\mathrm{bei}'\sqrt{p}}{\mathrm{ber}^2\sqrt{p} + \mathrm{bei}^2\sqrt{p}}\right) \tag{21b}$$

where $p = f/f_c$ is a dimensionless frequency parameter. An alternative, simpler presentation of the same formulation is shown by Butler and Lizza in Reference 216.

7.7. Dynamic Effects

As can be seen in Figure 9b and c, the resonant frequency of a Terfenol-D transducer varies significantly with operating conditions. The transducer mechanical resonance varies as a result of a number of factors. Some of these factors are the magnetostrictive core geometry, bias condition, delta E effect, AC magnetic field, external load, springs stiffness, and operating temperature. Other factors intrinsic to the specific design such as damping of internal components can also be significant.

The first mode axial resonance f_0 of a Terfenol-D transducer such as that sketched in Figure 1 is given by

$$f_0 = \frac{1}{2\pi}\sqrt{\frac{k_m + k_{ps}}{m_{eff}}} \tag{22}$$

where k_m is the magnetostrictive core stiffness, k_{ps} is the prestress mechanism stiffness, and m_{eff} is the system effective dynamic mass. The effective mass in the equation is formed by one-third of the mass of the rod plus the external load plus components of the prestress mechanism. Recognizing that the magnetostrictive material's compliance is strongly dependent upon operating conditions, the resonance frequencies of the device will be strongly dependent on operating conditions. Increasing AC magnetic field intensity increases the system compliance; hence, it decreases transducer resonant frequencies Figure 9b, while increasing prestress increases the system stiffness and hence resonant frequencies (Figure 9c). Control of the transducer resonant frequency over a range of 1200–1800 Hz using the delta E effect has been used in the design of magnetostrictive moving resonance or tunable vibration absorbers (217).

The dynamics of Terfenol-D transducers coupled to external loads are studied in Reference 218. An in-plane force-balancing model is used to consider both passive forces (those associated with the transducer and external load structural dynamics) and active forces (derived from the magnetostriction effect) to yield a PDE (partial differential equation) transducer model. The active component of the force is characterized by the strains predicted by the Jiles–Atherton ferromagnetic hysteresis model, combined with a magnetostriction quadratic law. The passive component is characterized by a PDE model of the transducer and external load structural mechanics. The model is capable of predicting the quasi-static magnetization state of the transducer core and of accurately predicting strains and displacements output by the transducer.

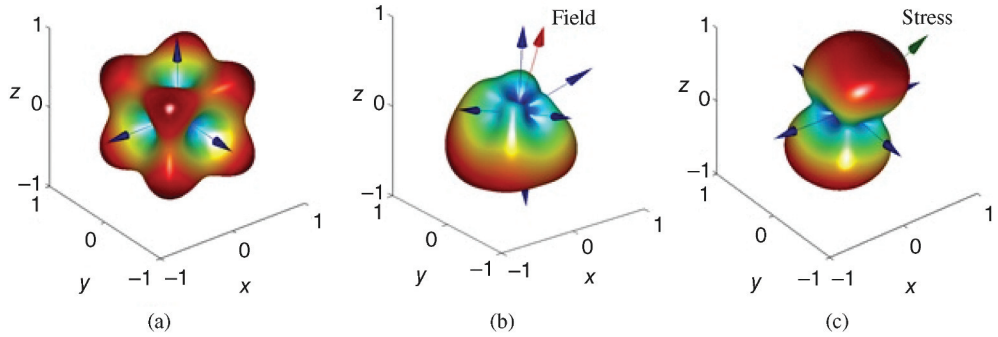

Figure 39. Gibbs energy equilibrium orientations with (a) no applied field or stress, (b) field only, and (c) stress only (213).

The parameter requirements of this model are minimal (experimental identification of six physically based parameters from quasi-static hysteresis loop measurements (e.g., saturation strain and magnetization)) and the model is computationally nondemanding given the relative simplicity of the underlying PDE system. Work is in progress to incorporate the effects of AC losses.

7.8. Finite-Element Approach

The models discussed previously are constructed on the assumption that either the applied magnetic field or the stress on the magnetostrictive materials is constant. However, practical magnetostrictive devices consist of active magnetostrictive materials as well as passive supporting components, such as coils, permanent magnets, and magnetic flux paths. The material and electrical properties of these components have the net effect of reducing the effective coupling efficiency of the device. The finite element model simulating magnetostrictive materials as well as passive surrounding components is a powerful tool for magnetostrictive system design. Previous studies have derived two-dimensional FE methods for magnetostrictive material systems, which are suitable for magnetostrictive systems with uniaxial magnetostriction and magnetization. The magnetostrictive effect was described through lookup tables that were derived either from experimental data (219,220) or from constitutive models (183,221,222). Shu et al. (104,223) recently incorporated a fully nonlinear constitutive model into the FE framework and achieved accurate simulation results up to 500 Hz.

Recent work has also successfully developed three-dimensional finite-element frameworks. Mudivarthi et al. (224) presented a 3D unidirectionally coupled FE model in a static regime on the basis of the Armstrong model. Evans and Dapino (225) built a 3D fully coupled FE model by neglecting the displacement currents, Lorentz forces, and voltage gradients in the magnetic domain. The framework was constructed on the basis of a piecewise linear assumption, and was later upgraded to fully nonlinear regimes by Chakrabarti and Dapino (105) through using an anhysteretic constitutive model (212). Deng and Dapino (226) recently incorporated the hysteresis property into previous FE model and successfully reproduced Galfenol stress–flux density minor loops under various bias conditions. All the FE models discussed above are in Cartesian coordinates. Taking advantage of the asymmetric rod geometry, studies have developed simplified FE models in cylindrical coordinates (80,179).

8. SUMMARY

This article first summarized the operation and historical context of magnetostrictive materials and then described typical material behavior and commonly used figures of merit. Several magnetostrictive device designs were discussed. The high strains and forces achievable with magnetostrictive transducers, high-coupling coefficients, and high-energy density of magnetostrictive materials have justified their use in an ever-increasing number of sensor and actuator applications, ranging from sonar projectors to vibration control, ultrasonics, and sensors designed to find corrosion in pipes. Magnetostrictive device performance capabilities are sometimes overlooked in the interest of avoiding nonlinear and hysteretic input–output transducer behaviors. The article presented selected energy-based constitutive models and finite-element system level models. Existing models are able to describe the material nonlinearities as well as multiphysics dynamics in their passive supporting components, such as electrical coils, magnets, and flux path.

BIBLIOGRAPHY

1. E. W. Lee. *Rep. Prog. Phys*. **1955**, *18*, 184–229.
2. E. Du Trémolet de Lacheisserie. *Magnetostriction: Magnetostriction Theory and Applications of Magnetoelasticity*. CRC Press, 1993.
3. F. V. Hunt and D. T. Blackstock. *Electroacoustics: The Analysis of Transduction and Its Historical Background*. American Institute of Physics for the Acoustical Society of America, 1982.
4. T. T. Hansen and T. A. Reinders. U.S. Patent 6,624,539 (to Edge Technologies, Inc.), 2003.
5. M. B. Moffett, R. Porzio, and G. L. Bernier. High-Power Terfenol-D Flextensional Transducer: Revision A. Technical Report, DTIC Document, 1995.
6. S. J. Hartman Magnetostrictive System for High-Frequency High-Cycle Fatigue Testing. Technical Report, University of Dayton Research Institute, 1997.
7. L. K. Jameson, B. Cohen, and L. H. Gipson. U.S. Patent 6,543,700 (to Kimberly-Clark Worldwide, Inc.), 2003.

8. Etrema Products, Inc. Available at //www.etrema.com/ (accessed November 16, 2015).
9. FeONIC. Available at http://www.feonic.com/ (accessed November 16, 2015).
10. P. D. McGary, L. Tan, J. Zou, B. J. Stadler, P. R. Downey, and A. B. Flatau. *J. Appl. Phys.* **2006**, *99*, p 08B310.
11. J. Weston, A. Butera, T. Lograsso, M. Shamsuzzoha, I. Zana, G. Zangari, and J. Barnard. *IEEE Trans. Magn.* **2002**, *38*, pp 2832–2834.
12. A. t. Clark and H. Belson. *Phys. Rev. B* **1972**, *5*, p 3642.
13. N. Koon, A. Schimdler, and F. Carter. *Phys. Lett. A* **1971**, *37*, pp 413–414.
14. R. Bozorth, *Ferromagnetism*. IEEE Press Classic Reissue, Wiley, 1993.
15. W. Corner and F. Hutchinson. *Proc. Phys. Soc.* **1958**, *72*, pp 1049–1052.
16. J. Cullen, A. Clark, M. Wun-Fogle, J. Restorff, and T. Lograsso. *J. Magn. Magn. Mater.* **2001**, *226*, pp 948–949.
17. M. Gibbs, P. Squires, P. Ford, and D. Brugel. *IEEE Trans. Magn.* **1988**, *24*, pp 1764–1766.
18. A. Clark, L. Kabacoff, H. Savage, and C. Modzelewski. U.S. Patent 4,763,030, 1988.
19. J. Butler. Magnetostrictive Transducer Design and Analysis. Technical Report, Image Acoustics, Inc., 1997.
20. Y. Lu and A. Nathan. *Appl. Phys. Lett.* **1997**, *70*, pp 526–528.
21. C. Body, G. Reyne, and G. Meunier. *J. Phys. III* **1997**, *7*, pp 67–85.
22. H. Uchida, M. Wada, A. Ichikawa, Y. Matsumura, and H. Uchida. *Proc. Actuator* **1996**, *96*, p 275.
23. T. Duenas, L. Hsu, and G. Cakman. *MRS Proc.* **1996**, *459*, p 527.
24. T. Cedell, *Magnetostrictive Materials and Selected Applications*. Lund Institute of Technology, 1995.
25. Y. Wu and M. A. Anjanappa. *Proc. SPIE.* **1996**, *2717*, pp 517–527.
26. P. Pulvirenti, D. Jiles, R. Greenough, and I. Reed. *J. Appl. Phys.* **1996**, *79*, pp 6219–6221.
27. E. Quandt. *J. Appl. Phys.* **1994**, *75*, pp 5653–5655.
28. M. Wun-Fogle, J. Restorff, and A. Clark. *J. Appl. Phys.* **1999**, *85*, pp 6253–6255.
29. R. D. James and M. Wuttig. *Phil. Mag. A* **1998**, *77*, pp 1273–1299.
30. M. Wuttig, L. Liu, K. Tsuchiya, and R. D. James. *J. Appl. Phys.* **2000**, *87*, pp 4707–4711.
31. A. E. Clark, M. Wun-Fogle, J. B. Restorff, and T. A. Lograsso. *Mater. Trans.* **2002**, *43*, pp 881–886.
32. T. V. Jayaraman, N. Srisukhumbowornchai, S. Guruswamy, and M. L. Free. *Corros. Sci.* **2007**, *49*, pp 4015–4027.
33. L. Dai, J. Cullen, M. Wuttig, T. Lograsso, and E. Quandt. *J. Appl. Phys.* **2003**, *93*, pp 8627–8629.
34. A. Nolting and E. Summers. *J. Mater. Sci.* **2015**, 50, pp 5136–5144.
35. A. E. Clark, T. A. Lograsso, and M. Wun-Fogle. U.S. Patent 11/822,778, 2007.
36. M. Huang, Y. Du, R. J. McQueeney, and T. A. Lograsso. *J. Appl. Phys.* **2010**, *107*, p 053520.
37. A. Clark, M. Wun-Fogle, J. Restorff, T. A. Lograsso, and G. Petculescu. *J. Appl. Phys.* **2004**, *95*, pp 6942–6944.
38. J. J. Scheidler, V. M. Asnani, Z. Deng, and M. J. Dapino. *Proc. SPIE* **2015**, *9432*, pp 94320J–94320J.
39. R. Kornbluh, R. Pelrine, Q. Pei, S. Oh, and J. Joseph. *Proc. SPIE* **2000**, *3987*. doi:10.1117/12.387763.
40. G. Engdahl. *Handbook of Giant Magnetostrictive Materials*.' Academic Press: San Diego, 2000.
41. D. L. Hall. Dynamics and Vibrations of Magnetostrictive Transducers. PhD thesis, Iowa State University, 1994.
42. E. Summers, R. Meloy, and J. Restorff. *J. Appl. Phys.* **2009**, *106*, pp 024914–024914.
43. F. A. Fischer. *Fundamentals of Electroacoustics*. Interscience Publishers, 1955.
44. K. D. Rolt. *J. Acoust. Soc. Am.* **1990**, *87*, pp 1340–1349.
45. U.S. Office of Scientific Research and Development, National Defence Research Committee. The Design and Construction of Magnetostriction Transducers. Summary Technical Report of the National Defense Research Committee, Summary Technical Report of Division 6, NDRC: Washington, DC, 1946.
46. M. B. Moffett, J. M. Powers, and A. E. Clark. *J. Acoust. Soc. Am.* **1991**, *90*, pp 1184–1185.
47. M. B. Moffett and W. L. Clay, Jr. *J. Acoust. Soc. Am.* **1993**, *93*, pp 1653–1654.
48. T. Akutsu. An Application of Giant Magnetostrictive Material to High Power Actuators, in *Proc. 10th International Workshop on Rare-Earth Magnets and Their Applications*, 1989.
49. S. Datta, J. Atulasimha, and A. B. Flatau. *J. Magn. Magn. Mater.* **2009**, *321*, pp 4017–4031.
50. M. J. Dapino, A. B. Flatau, and F. T. Calkins. *J. Intell. Mater. Syst. Struct.* **2006**, *17*, pp 587–599.
51. M. J. Dapino, F. T. Calkins, A. B. Flatau, and D. L. Hall. Measured Terfenol-D Material Properties under Varied Applied Magnetic Field Levels, in *Proc. SPIE Symposium on Smart Structures and Materials*; International Society for Optics and Photonics, 1996, pp 697–708.
52. M. B. Moffett, A. E. Clark, M. Wun-Fogle, J. Linberg, J. P. Teter, and E. A. McLaughlin. *J. Acoust. Soc. Am.* **1991**, *89*, pp 1448–1455.
53. F. T. Calkins, M. J. Dapino, and A. B. Flatau. Effect of Prestress on the Dynamic Performance of a Terfenol-D Transducer, in *Proc. SPIE Symposium on Smart Structures and Materials*; International Society for Optics and Photonics, 1997, pp 293–304.
54. J. L. Butler. *Application Manual for the Design of ETREMA Terfenol-D Magnetostrictive Transducers*. Etrema Products, Inc., 1988.
55. M. Rossi and P. R. W. Roe. *Acoustics and Electroacoustics*, vol. 685; Artech House: Norwood, MA, 1988.
56. F. T. Calkins and A. B. Flatau. Transducer-Based Measurements of Terfenol-D Material Properties, in *Proc. SPIE Symposium on Smart Structures and Materials*; International Society for Optics and Photonics, 1996, pp 709–719.
57. A. Clark. *Magnetostrictive Rare Earth-Fe2 Compounds*. Springer, 1988.
58. M. Dapino. Nonlinear and Hysteretic Magnetomechanical Model for Magnetostrictive Transducers. PhD dissertation, Iowa State University, 1999.
59. V. Giurgiutiu. *Micromechatronics: Modeling, Analysis, and Design with MATLAB* 2nd ed.; CRC Press, 2009.
60. M. B. Moffett. *J. Acoust. Soc. Am.* **1993**, *94*, pp 3503–3505.
61. R. Woollett. *Ultrasonics* **1969**, *7*, p 84.
62. F. T. Calkins. Design, Analysis, and Modeling of Giant Magnetostrictive Transducers. PhD thesis, Iowa State University, 1997.

63. F. Claeyssen et al. Progress in Magnetostrictive Sonar Transducers, in *Proc. Undersea Defence Technology Conference (UDT93)*; Reed Exhibition Companies, UK, 1993, pp 246–250.
64. H. C. Hayes. U.S. Patent 2,064,911, 1936.
65. W. J. Toulis. U.S. Patent 3,274,537, 1966.
66. L. H. Royster. *Appl. Acoust.* **1970**, *3*, pp 117–126.
67. G. A. Brigham and L. H. Royster. *J. Acoust. Soc. Am.* **1969**, *46*, pp 92–92.
68. H. C. Merchant. U.S. Patent 3,258,738 (to Honeywell Inc.), 1966.
69. E. Rynne. Innovative Approaches for Generating High Power, Low Frequency Sound, in *Proc. Transducers for Sonics and Ultrasonics*; 1993, pp 38–49.
70. F. R. Abbott. U.S. Patent 2,895,062, 1959.
71. D. R. E. Atlantic and C. Purcell. *Terfenol Driver for the Barrel-Stave Projector*. Defence Research Establishment Atlantic, 1992.
72. D. Jones. Flextensional Barrel-Stave Projectors, in *Transducers for Sonics and Ultrasonics*; 1992, pp 150–159.
73. J. Pagliarini and R. White. A Small Wide-Band, Low-Frequency, High-Power Sound Source Utilizing the Flextensional Transducer Concept, in *Proc. Oceans Engineering for Today's Technology and Tomorrow's Preservation* (*OCEANS'78)*; IEEE, 1978, pp 333–338.
74. J. Debus, J. Decarpigny, and B. Hamonic. Analysis of a Class IV Flextensional Transducer Using Piece-Part Equivalent Circuit Models, in *Transducers for Sonics and Ultrasonics*; 1992, pp 181–197.
75. F. Claeyssen, N. Lhermet, and G. Grosso. *J. Appl. Electromagn. Mater.* **1993**, *5*, pp 67–73.
76. G. Steel. A 2 khz Magnetostrictive Transducer, in *Transducers for Sonics and Ultrasonics*; 1992, p 258.
77. S. Butler and J. Lindberg. A Broadband Hybrid Magnetostrictive/Piezoelectric Tonpilz Transducer, in *Proc. UDT 98*; Sydney, Australia, 1998.
78. S. Meeks and R. Timme. *J. Acoust. Soc. Am.* **1977**, *62*, pp 1158–1164.
79. F. Claeyssen and D. Boucher. Design of Lanthanide Magnetostrictive Sonar Projectors, in *Proc. UDT*; Paris, France, 1991, pp 1059–1065.
80. S. Chakrabarti and M. J. Dapino. *Smart Mater. Struct.* **2010**, *19*, p 055009.
81. S. Chakrabarti and M. J. Dapino. *Proc. SPIE*, **2010**, *7645*, pp 76450G–76450G.
82. H. C. Hayes. U.S. Patent 2,005,741, 1935.
83. S. L. Ebrlich. U.S. Patent 3,290,646 (to Raytheon Co.), 1966.
84. S. M. Cohick and J. L Butler. *J. Acoust. Soc. Am.* **1982**, *72*, pp 313–315.
85. J. Butler and S. Ciosek. *J. Acoust. Soc. Am.* **1980**, *67*, pp 1809–1811.
86. R. L. Zrostlik, D. L. Hall, and A. B. Flatau. Analog and Digital Feedback for Magnetostrictive Transducer Linearization, in *Proc. SPIE Symposium on Smart Structures and Materials*, International Society for Optics and Photonics, 1996, pp 578–587.
87. M. D. Bryant, B. Fernandez, N. Wang, V. V. Murty, V. Vadlamani, and T. S. West. *J. Intell. Mater. Syst. Struct.* **1993**, *4*, pp 484–489.
88. J. R. Pratt and A. H. Nayfeh. Smart Structures for Chatter Control, in *Proc. SPIE 5th Annual International Symposium Smart Structures and Materials*; International Society for Optics and Photonics, 1998, pp 161–172.
89. T. Fujita, H. Nonaka, C. S. Yang, H. Kondo, Y. Mori, and Y. Amasaka. Active Vibration Control of Frame Structures with a Smart Structure Using Magnetostrictive Actuators, in *Proc. SPIE 5th Annual International Symposium Smart Structures and Materials*; International Society for Optics and Photonics, 1998, pp 584–595.
90. L. D. Jones and E. Garcia. Application of the Self-Sensing Principle to a Magnetostrictive Structural Element for Vibration Suppression, in *Proc. ASME International Mechanical Engineering Congress and Exposition*; 1994, vol. 45, pp 155–155.
91. L. Kiesewetter. The Application of Terfenol in Linear Motors, in *Proc. 2nd International Conference on Giant Magnetostrictive Alloys*, 1988, p 15.
92. R. Roth. The Elastic Wave Motor-A Versatile Terfenol Driven, Linear Actuator with High Force and Great Precision, in *Proc. International Intelligent Motion*; Intertec International Inc., 1992, p 1.
93. F. Austin, M. J. Siclari, M. Kesselman, and G. N. Weisensel. Smart Terfenol-D-Powered Trailing-Edge Experiment, in *Proc. SPIE 5th Annual International Symposium on Smart Structures and Materials*; International Society for Optics and Photonics, 1998, pp 282–293.
94. Z. G. Zhang, T. Ueno, and T. Higuchi. *IEEE Trans. Magn.* **2009**, *45*, pp 4598–4600.
95. J. E. Miesner and J. P. Teter. Piezoelectric/Magnetostrictive Resonant Inchworm Motor, in *Proc. SPIE Symposium on Smart Structures and Materials*; International Society for Optics and Photonics, 1994, pp 520–527.
96. B. Clephas and H. Janocha. New Linear Motor with a Hybrid Actuator, in *Proc. SPIE Symposium on Smart Structures and Materials*; International Society for Optics and Photonics, 1997, pp 316–325.
97. L. Kvarnsjö, On Characterization, Modelling and Application of Highly Magnetostrictive Materials. PhD thesis, Royal Institute of Technology, Sweden, 1993.
98. T. Akutsu. *Proc. Actuators*, **1992**, *92*, pp 244–248.
99. J. Vranish, D. Naik, J. Restorff, and J. Teter. *IEEE Trans. Magn.* **1991**, *27*, pp 5355–5357.
100. F. Claeyssen, N. Lhermet, R. Le Letty, and L. Chouteau. A New Resonant Magnetostrictive Rotating Motor, in *Proc. 5th International Conference on New Actuators, Bremen*; 1996, p 272.
101. T. Ueno, C. Saito, N. Imaizumi, and T. Higuchi. *Sens. Actuators A* **2009**, *154*, pp 92–96.
102. R. Venkataraman. A Hybrid Actuator. Technical Report, DTIC Document, 1995.
103. A. Krishna Murty, M. Anjanappa, and Y.-F. Wu. *J. Sound Vib.* **1997**, *206*, pp 133–149.
104. L. Shu, L. M. Headings, M. J. Dapino, D. Chen, and Q. Lu. *J. Intell. Mater. Syst. Struct.* **2014**, *25*, pp 187–203.
105. S. Chakrabarti and M. J. Dapino. *Smart Mater. Struct.* **2011**, *20*, p 105034.
106. J. Kumar, N. Ganesan, S. Swarnamani, and C. Padmanabhan. *J. Sound Vib.* **2003**, *262*, pp 577–589.
107. J. R. Frederick. *Ultrasonic Engineering*. John Wiley & Sons, Inc., 1965.
108. G. Gooberman. *Ultrasonics: Theory and Application*, Science and Technology Series. Hart Publishing Company, 1969.
109. J. Szilard. *Encyclopedia of Physical Science and Technology*, vol. 17, **1992,** pp 153–173.

110. T. Hansen. *CHEMTECH* **1996**, *26*, pp 56–59.
111. A. Markov, *Ultrasonic Machining of Intractable Materials*. Iliffe Books Limited, 1966.
112. H. E. Bass. *Encyclopedia of Science and Technology*, 8th ed.; McGraw-Hill: New York, 1977.
113. N. A. Technol. Development of Terfenol-D High-Powered Ultrasonic Transducer Technology for Sonochemistry. Technical Report NIST Grant No. 97-01-0023, December 2000.
114. S. Ueha, Y. Tomikawa, M. Kurosawa, and N. Nakamura. *Ultrasonic Motors: Theory and Applications*. Clarendon Press: Oxford, 1993.
115. F. Claeyssen, R. Le Letty, F. Barillot, J. Betz, K. MacKay, D. Givord, and P. Bouchilloux. Micromotors Using Magnetostrictive Thin Films, in *Proc. SPIE 5th Annual International Symposium on Smart Structures and Materials*; International Society for Optics and Photonics, 1998, pp 786–793.
116. S. R. Day, G. Raghunath, S. J. Stebbins, S. M. Na, A. B. Flatau, and R. A. Swartz. On-Going Testing of Prototype Full-Scale, Bio-Inspired Scour Monitoring Systems, in *Proc. 6th World Conference on Structural Control and Monitoring,* vol. 2, 2014.
117. S. M. Na and A. B. Flatau. *J. Appl. Phys.* **2014**, *115*, pp 17A93.
118. G. Raghunath, A. B. Flatau, S. M. Na, and B. Barkely. Development of a Bio-Inspired Tactile Magnetostrictive Whisker Sensor Using Alfenol, in *Proc. SMASIS.*, 2014.
119. D. M. Dozor. Magnetostrictive Wire-Bonding Clamp for Semiconductor Packaging: Initial Prototype Design, Modeling, and Experiments, in *Proc. 5th SPIE Annual International Symposium on Smart Structures and Materials*; International Society for Optics and Photonics, 1998, pp 516–526.
120. O. D. Brimhall and C. J. Hasser. Magnetostrictive Linear Devices for Force Reflection in Dexterous Telemanipulation, in *1994 North American Conference on Smart Structures and Materials*; International Society for Optics and Photonics, **1994**, pp 508–519.
121. B. Mersky and V. P. Thompson. U.S. Patent 5,460,593 (to Audiodonics, Inc.), 1995.
122. R. Cutler, G. E. Sleefe, and R. G. Keefe. Development of a Magnetostrictive Borehole Seismic Source. Technical Report, Sandia National Labs, Albuquerque, NM, 1997.
123. G. A. Hartman and J. R. Sebastian. U.S. Patent 5,719,339 (to the University of Dayton), 1998.
124. J. Restorff. *Encyclopedia of Applied Physics* **1994**, *9*, pp 229–244.
125. R. Kellogg and A. B. Flatau. *J. Intell. Mater. Syst. Struct.* **2007**, *19*, pp 583–585.
126. S. Datta, J. Atulasimha, C. Mudivarthi, and A. Flatau. *J. Magn. Magn. Mater.* **2010**, *322*, pp 2135–2144.
127. J. J. Scheidler and M. J. Dapino. *Smart Mater. Struct.* **2013**, *22*, p 085015.
128. J. Scheidler, M. Dapino, and V. Asnani. Dynamic Characterization of Galfenol(Fe81:6Ga18:4). Technical Report, NASA Glenn Research Center, 2015.
129. S. Dong, J.-F. Li, and D. Viehland. *Appl. Phys. Lett.* **2004**, *85*, pp 2307–2309.
130. W. J. Fleming. Magnetostrictive Torque Sensors: Comparison of Branch, Cross, and Solenoidal Designs. Technical Report, SAE Technical Paper, 1990.
131. W. J. Fleming. Magnetostrictive Torque Sensor Performance: Nonlinear Analysis, in *IEEE 39th Conference on Vehicular Technology*; IEEE, 1989, pp 413–422.
132. J. Yamasaki, K. Mohri, T. Manabe, N. Teshima, and S. Fukuda. *IEEE Trans. Magn.* **1986**,*22*, pp 403–405.
133. K. Mohri. *IEEE Trans. Magn.* **1984**, *20*, pp 942–947.
134. I. Sasada, S. Uramoto, and K. Harada. *IEEE Trans. Magn.* **1986**, *22*, pp 406–408.
135. I. J. Garshelis. *IEEE Trans. Magn.* **1993**, *29*, pp 3201–3203.
136. I. J. Garshelis and C. R. Conto. *IEEE Trans. Magn.* **1994**, *30*, pp 4629–4631.
137. A. Mahadevan. Force and Torque Sensing with Galfenol Alloys. PhD thesis, the Ohio State University, 2009.
138. I. Sasada, N. Suzuki, T. Sasaoka, and K. Toda. *IEEE Trans. Magn.* **1994**, *30*, pp 4632–4634.
139. M. Shimada. *J. Appl. Phys.* **1993**, *73*, pp 6872–6874.
140. J. Pratt and A. B. Flatau. *J. Intell. Mater. Syst. Struct.* **1995**, *6*, pp 639–648.
141. J. R. Pratt. Design and Analysis of a Self-Sensing Terfenol-D Magnetostrictive Actuator. PhD thesis, Iowa State University, 1993.
142. R. C. Fenn and M. J. Gerver. Passive Damping and Velocity Sensing Using Magnetostrictive Transduction, in *1994 North American Conference on Smart Structures and Materials*; International Society for Optics and Photonics, 1994, pp 216–227.
143. D. K. Kleinke and H. M. Uras. *Rev. Sci. Instrum.* **1993**, *64*, pp 2361–2367.
144. D. Nyce. *Sens. J. Appl. Sensing Technol.* **1994**, *11*, pp 22–26.
145. J. Peyrucat. *Mesures* 1986, *43*, p 16.
146. M. Wun-Fogle, H. Savage, and M. Spano. *J. Mater. Eng.* **1989**, *11*, pp 103–107.
147. E. Hristoforou and R. Reilly. *IEEE Trans. Magn.* **1994**, *30*, pp 2728–2733.
148. J.-H. Yoo, U. Marschner, and A. B. Flatau. Preliminary Galfenol Vibratory Gyro-Sensor Design, in *Proc. SPIE Symposium on Smart Structures and Materials*; International Society for Optics and Photonics, 2005, pp 111–119.
149. U. Marschner, F. Graham, C. Mudivarthi, J.-H. Yoo, H. Neubert, and A. Flatau. *J. Appl. Phys.* **2010**, *107*, p 09E705.
150. E. Hristoforou and R. Reilly. *IEEE Trans. Magn.* **1992**, *28*, pp 1974–1977.
151. R. E. Reilly. U.S. Patent 4,924,711 (to National Research Development Corporation), 1990.
152. L. Weng, T. Walker, Z. Deng, M. Dapino, and B. Wang. *J. Appl. Phys.* **2013**, *113*, p 024508.
153. P. Evans and M. Dapino. *J. Appl. Phys.* **2010**, *108*, pp 074517–074517.
154. D. K. Kleinke and H. M. Uras. *Rev. Sci. Instrum.* **1994**, *65*, pp 1699–1710.
155. M. H. Uras. U.S. Patent 6,622,577, 2003.
156. T. A. Baudendistel and M. L. Turner. *IEEE Sens. J.* **2007**, *7*, pp 245–250.
157. J. Seekircher and B. Hoffmann. *Sens Actuators A Phys.* **1989**, *22*, pp 401–405.
158. E. Orsier, A. Garnier, T. Hiramoto, H. Fujita, J. Betz, K. MacKay, J.-C. Peuzin, and D. Givord. Contactless Actuation of Giant Magnetostriction Thin-Film Alloy Bimorphs for Two-Dimensional Scanning Application, in *Micromachining*

and Microfabrication, International Society for Optics and Photonics, 1997, pp 98–108.

159. K. Mohri and S. Takeuchi. *IEEE Trans. Magn.* **1981**, *17*, pp 3379–3381.
160. J. Zakrzewski. *IEEE Trans. Instrum. Meas.* **1997**, *46*, pp 807–810.
161. K. A. Bartels, H. Kwun, and J. J. Hanley. Magnetostrictive Sensors for the Characterization of Corrosion in Rebars and Prestressing Strands, in *Nondestructive Evaluation Techniques for Aging Infrastructure and Manufacturing*; International Society for Optics and Photonics, 1996. pp 40–50.
162. H. Kwun and M. T. I. Cecil. U.S. Patent 5,581,037 (to Southwest Research Institute), 1996.
163. J. Brophy and C. R. Brett. Guided at Wave Inspection of Insulated Feedwater Piping Using Magnetostrictive Sensors, in *Nondestructive Evaluation Techniques for Aging Infrastructure and Manufacturing*; International Society for Optics and Photonics, 1996, pp 205–210.
164. G. P. Carman and M. Mitrovic. *J. Intell. Mater. Syst. Struct.* **1995**, *6*, pp 673–683.
165. Y. Kim and Y. Y. Kim. *Sens. Actuators* **2007**, *133*, pp 447–456.
166. X. Wang, J. Zou, F. Wang, and R. Li. *Sens. Transducers J.* **2013**, *159*, p 450.
167. S. Foner. *IEEE Trans. Magn.* **1981**, *17*, pp 3358–3363.
168. R. Weber, D. Jiles, U.S. Department of Commerce, and Iowa State University. Center for Advanced Technology Development, *A Terfenol-D Based Magnetostrictive Diode Laser Magnetometer*, Center for Advanced Technology Development, Iowa State University, 1992.
169. R. Chung, R. Weber, and D. Jiles. *IEEE Trans. Magn.* **1991**, *27*, pp 5358–5360.
170. J. F. Doherty, S. Arigapudi, and R. Weber. *IEEE Trans. Magn.* **1994**, *30*, pp 1274–1290.
171. J. Zhai, S. Dong, Z. Xing, J. Li, and D. Viehland. *Appl. Phys. Lett.* **2007**, *91*, p 123513.
172. A. Yariv and H. V. Winsor. *Opt. Lett.* **1980**, *5*, pp 87–89.
173. M. Mermelstein. *Electron. Lett.* **1985**, *21*, pp 1178–1179.
174. E. Hristoforou, H. Chiriac, and M. Neagu. *IEEE Trans. Instrum. Meas.* **1997**, *46*, pp 632–635.
175. S. M. Quintero, A. Braga, H. I. Weber, A. C. Bruno, and J. F. Araújo. *Sensors* **2010**, *10*, pp 8119–8128.
176. Y. Torii, H. Wakiwaka, T. Kiyomiya, Y. Matsuo, Y. Yamada, and M. Makimura. *J. Magn. Magn. Mater.* **2005**, *290*, pp 861–864.
177. C. Wenzel, B. Adolphi, U. Merkel, A. Jahn, U. Marschner, J. Ziske, H. Neubert, and W.-J. Fischer. *Sens Actuators A Phys.* **2009**, *156*, pp 129–133.
178. S. Sauer, U. Marschner, B. Adolphi, B. Clasbrummel, and W. Fischer. *IEEE Sens. J.* **2012**, *12*, pp 1226–1233.
179. Z. Deng, V. M. Asnani, and M. Dapino. Magnetostrictive Vibration Damper and Energy Harvester for Rotating Machinery, in *Proc. SPIE 9433*, International Society for Optics and Photonics, 2015, pp 94330C–94330C.
180. W. J. Pulliam, D. Lee, G. P. Carman, and G. P. McKnight. Thin-Layer Magnetostrictive Composite Films for Turbomachinery Fan Blade Damping, in *Proc. SPIE Symposium on Smart Structures and Materials*, International Society for Optics and Photonics, 2003, pp 360–371.
181. A. J. Murray and J. Yoo. Evaluation of Magnetostrictive Shunt Damper Performance Using Iron (Fe)-Gallium (Ga) Alloy. Technical Report, DTIC Document, 2013.
182. V. Berbyuk. Vibration Energy Harvesting Using Galfenol-Based Transducer, in *Proc. SPIE 8688*, International Society for Optics and Photonics, 2013, pp 86881F–86881F.
183. Z. Deng and M. J. Dapino. *Smart Mater. Struct.* **2015**, *24*, p 125019.
184. L. Wang and F. Yuan. *Smart Mater. Struct.* **2008**, *17*, p 045009.
185. T. Ueno and S. Yamada. *IEEE Trans. Magn.* **2011**, *47*, pp 2407–2409.
186. T. Meydan and M. Elshebani. *IEEE Trans. Magn.* **1991**, *27*, pp 5250–5252.
187. T. Worthington, P. Calcagno, L. Romankiw, and D. Thompson. *IEEE Trans. Magn.* **1979**, *15*, pp 1797–1799.
188. K. Shirae and A. Honda. *IEEE Trans. Magn.* **1981**, *17*, p 31511.
189. T. Klinger, H. Pfutzner, P. Schonhuber, K. Hoffmann, and N. Bachl. *IEEE Trans. Magn.* **1992**, *28*, pp 2400–2402.
190. P. G. Stoyanov and C. A. Grimes. *Sens. Actuators A Phys.* **2000**, *80*, pp 8–14.
191. S. Sang, P. Cheng, W. Zhang, P. Li, J. Hu, G. Li, and A. Jian. *J. Intell. Mater. Syst. Struct.* **2014**. doi: 1045389X14544139.
192. T. Klinger, F. Schmollebeck, H. Pfutzner, and P. Schonhuber. *IEEE Trans. Magn.* **1992**, *28*, pp 2397–2399.
193. K. Kannan and A. Dasgupta. Continuum Magnetoelastic Properties of Terfenol-D What Is Available and What Is Needed, in Proc. *ASME Adaptive Materia Symposium*, vol. *206*, Summer Meeting, Division Publications AMD, 1995, pp 141–141.
194. J. Restorff, H. Savage, A. Clark, and M. Wun-Fogle. *J. Appl. Phys.* **1990**, *67*, pp 5016–5018.
195. A. Adly and I. Mayergoyz. *IEEE Trans. Magn.* **1996**, *32*, pp 4773–4775.
196. R. C. Smith. Modeling Techniques for Magnetostrictive Actuators, in *Proc. SPIE Symposium on Smart Structures and Materials*, International Society for Optics and Photonics, 1997, pp 243–253.
197. G. Engdahl and A. Bergqvist. *J. Appl. Phys.* **1996**, *79*, pp 4689–4691.
198. V. Basso and G. Bertotti. *IEEE Trans. Magn.* **1996**, *32*, pp 4210–4212.
199. W. F. Brown, *Magnetoelastic Interactions*, vol. 9; Springer, 1966.
200. R. D. James and D. Kinderlehrer. *Phil. Mag. B* **1993**, *68*, pp 237–274.
201. A. Reimers and E. Della Torre. *IEEE Trans. Magn.* **1998**, *34*, pp 3857–3866.
202. E. C. Stoner and E. Wohlfarth. *Philos. Trans. R. Soc. Lond. A. Math. Phys. Sci.* **1948**, *20*, pp 599–642.
203. E. Lee and J. Bishop. *Proc. Phys. Soc.* **1966**, *89*, p 661.
204. A. Clark, H. Savage, and M. Spano. *IEEE Trans. Magn.* **1984**, *20*, pp 1443–1445.
205. D. Jiles and J. Thoelke. *J. Magn. Magn. Mater.* **1994**, *134*, pp 143–160.
206. D. Jiles and D. Atherton. *J. Magn. Magn. Mater.* **1986**, *61*, pp 48–60.
207. A. Clark, J. Teter, M. Wun-Fogle, M. Moffett, and J. Lindberg. *J. Appl. Phys.* **1990**, *67*, pp 5007–5009.
208. C. L. Hom and N. Shankar. *J. Intell. Mater. Syst. Struct.* **1994**, *5*, pp 795–801.
209. I. D. Mayergoyz. *The Classical Preisach Model of Hysteresis*. Springer, 1991.

210. M. Al Janaideh, S. Rakheja, and C.-Y. Su. *Smart Mater. Struct.* **2009**, *18*, p 045001.
211. W. D. Armstrong. *J. Appl. Phys.* **1997**, *81*, pp 2321–2326.
212. P. Evans and M. Dapino. *J. Appl. Phys.* **2010**, *107*, pp 063906–063906.
213. P. G. Evans and M. J. Dapino. Fully-Coupled Magnetoelastic Model for Galfenol Alloys Incorporating Eddy Current Losses and Thermal Relaxation, in *Proc. SPIE 6929*, International Society for Optics and Photonics, 2008, pp 69291W–69291W.
214. W. D. Armstrong. *J. Magn. Magn. Mater.* **2003**, *263*, pp 208–218.
215. D. Jiles. *J. Appl. Phys.* **1994**, *76*, pp 5849–5855.
216. J. L. Butler and N. L. Lizza. *J. Acoust. Soc. Am.* **1987**, *82*, pp 378–378.
217. A. B. Flatau, M. J. Dapino, and F. T. Calkins. High Bandwidth Tunability in a Smart Vibration Absorber, in *Proc. 5th Annual International Symposium* on *Smart Structures and Materials*, International Society for Optics and Photonics, 1998, pp 463–473.
218. M. J. Dapino, R. C. Smith, and A. B. Flatau. Active and Structural Strain Model for Magnetostrictive Transducers, in *Proc. 5th Annual International Symposium on Smart Structures and Materials*, International Society for Optics and Photonics, 1998, pp 198–209.
219. M. E. H. Benbouzid, R. Beguenane, G. Reyne, and G. Meunier. Finite Element Modeling of Terfenol-D Magneto-Mechanical Coupling: Application to a Direct Micro-Stepping Rotary Motor, in *1997 IEEE International Electric Machines and Drives Conference Record*, IEEE, 1997, pp WC2–WC6.
220. K. Kannan and A. Dasgupta. *Smart Mater. Struct.* **1997**, *6*, p 341.
221. Z. Deng and M. Dapino. *J. Intell Mater. Syst. Struct.* **2015**. In review.
222. B. Rezaeealam, T. Ueno, and S. Yamada. *IEEE Trans. Magn.* **2012**, *48*, pp 3977–3980.
223. L. Shu, M. J. Dapino, P. G. Evans, D. Chen, and Q. Lu. *J. Intell Mater. Syst. Struct.* **2011**, *22*, pp 781–793.
224. C. Mudivarthi, S. Datta, J. Atulasimha, and A. Flatau. *Smart Mater. Struct.* **2008**, *17*, p 035005.
225. P. G. Evans and M. J. Dapino. *IEEE Trans. Magn.* **2011**, *47*, pp 221–230.
226. 226. Z. Deng and M. Dapino. *J. Intell. Mater. Syst. Struct.* **2015**, *26*, pp 47–55.

MARCELO J. DAPINO,
ZHANGXIANG DENG
Ohio State University,
Columbus, OH, USA

FREDERICK T. CALKINS
Boeing, Seattle, WA, USA

ALISON B. FLATAU
University of Maryland College
Park, MD, USA